Wnt target IQGAP3 promotes Wnt signaling via disrupting Axin1-CK1α interaction.

Muhammad Bakhait Rahmat[1, *], Aashiq Hussain[1], Teh Yu Xuan[1], Bibek Dutta[1], Sumedha Pundrik[1], Dennis Kappei[1,2,3], Yoshiaki Ito[1, *]

[1]Cancer Science Institute of Singapore, National University of Singapore, Singapore.

[2]Department of Biochemistry, Yong Loo Lin School of Medicine, National University of Singapore, Singapore

[3]NUS Center for Cancer Research, Yong Loo Lin School of Medicine, National University of Singapore, Singapore

*Correspondence:

Yoshiaki Ito, Cancer Science Institute of Singapore, NUS Centre for Cancer Research, Yong Loo Lin School of Medicine, National University of Singapore, 14 Medical Drive #12-01, Singapore 117599.

Tel: +65-6516-2242, Fax: +65-6873-9664, email: yoshi_ito@nus.edu.sg.

Muhammad Bakhait Rahmat, email: csimbr@nus.edu.sg or bhitihd@hotmail.com.

ABSTRACT

The scaffold protein IQGAP3 is highly upregulated in most epithelial cancers. While recent studies have highlighted its pivotal roles in cancer cell proliferation and metastasis, a deeper mechanistic understanding of IQGAP3 is currently lacking. We have here used TurboID to map IQGAP3 proximity partners and identified the Wnt signaling members Axin1 and CK1α as IQGAP3-interacting proteins. Our functional studies demonstrated that overexpression of IQGAP3 increases β-catenin levels, while IQGAP3 depletion reduces β-catenin levels in gastric cancer cells. Mechanistically, IQGAP3 disrupts Axin1-CK1α interaction, thereby inhibiting β-catenin phosphorylation and ultimately leading to its accumulation. Importantly, we discovered that IQGAP3 itself is regulated by Wnt signaling, suggesting its involvement in a positive feedback loop in Wnt/β-catenin signaling through interactions with Axin1 and CK1α. These findings identify IQGAP3 as a novel mediator of β-catenin stabilization and underscore its potential as a target for cancer therapy.

31 **INTRODUCTION**

32 IQ motif GTPase-activating scaffold proteins (IQGAPs) belong to a family of scaffold proteins,
33 which facilitates physical interactions between effector proteins to coordinate signaling
34 pathways involved in cytoskeleton dynamics (Brandt & Grosse, 2007, Wang, Watanabe et al.,
35 2007), cell proliferation (Nojima, Adachi et al., 2008), and cytokinesis (Adachi, Kawasaki et al.,
36 2014). The mammalian IQGAP family consists of three proteins: IQGAP1, IQGAP2, and IQGAP3.
37 The prevalence of IQGAP1 and IQGAP3 in multiple cancer types indicates fundamental roles in
38 tumorigenesis (Sanchez-Laorden, Viros et al., 2013), indeed, IQGAP1 and 3 have been established
39 as potential targets for cancer therapy (Monteleon, McNeal et al., 2015).
40
41 IQGAP3 is located on chromosome 1q21.3, which is frequently amplified in many malignant
42 tumors (Goh, Feng et al., 2017, Vazquez-Mena, Medina-Martinez et al., 2012). Amongst the
43 IQGAP family, IQGAP3 alone is necessary and sufficient for driving cell proliferation (Nojima et
44 al., 2008). Moreover, *Iqgap3* is specifically expressed in proliferating stomach stem cells and
45 regenerating stomach tissues in the mouse (Matsuo, Douchi et al., 2021). The robust elevation
46 of Iqgap3 following tissue injury is indicative of a requirement for IQGAP3 during wound healing
47 (Matsuo et al., 2021). Injury-induced *Iqgap3* expression is associated upregulation of *Myc* gene
48 targets, embryonic stem cell-like transcriptional signature and importantly, transcriptional
49 programs associated with early gastric cancer (Matsuo, Douchi et al., 2020). More recently, the
50 identification of oncofetal protein IGF2BP1 as a regulator of *IQGAP3* RNA stability suggests that
51 fetal-like reprogramming in tumors led to IQGAP3 overexpression and hyperproliferation of
52 stem-like cancer cells (Myint, Chuang et al., 2022). Mechanistically, IQGAP3 serves as an
53 important hub for multiple oncogenic signaling pathways: PI3K/AKT (Lin, Liu et al., 2019),
54 MAPK/ERK (Nojima et al., 2008, Yang, Zhao et al., 2014) and Wnt/β-catenin (Carmon, Gong et al.,
55 2014). Understanding how IQGAP3 influences these pathways will help the design of effective
56 strategies to inhibit proliferation and promote terminal differentiation in the 'wound that does
57 not heal' – cancer.
58
59 Uncontrolled proliferation is a hallmark of cancer, driven by dysregulated signaling pathways that
60 often involve scaffold and adaptor proteins to ensure precise spatiotemporal coordination.

61 Recent findings highlight the role of biomolecular condensates formed via liquid-liquid phase
62 separation (LLPS) as a key mechanism for coordinating intracellular processes (Mehta & Zhang,
63 2022, Nesterov, Ilyinsky et al., 2021, Tong, Tang et al., 2022), including cancer-related signaling
64 (Hu, Wu et al., 2023, Meng, Yu et al., 2021). Proteins within LLPS function as scaffolds, driving
65 phase separation, or clients, integrating into condensates to enhance multivalent interactions for
66 efficient signal transduction (Banani, Rice et al., 2016). Wnt signaling, crucial for cell proliferation,
67 differentiation, and stem cell maintenance, is frequently dysregulated in cancer, leading to β-
68 catenin stabilization, overexpression of target genes (e.g., *MYC*, *CCND1*, *LGR5*) (Ramakrishnan &
69 Cadigan, 2017), and subsequent tumor growth and metastasis. The β-catenin destruction
70 complex, composed of Axin, APC, GSK3β, and CK1α, regulates β-catenin levels, with Axin's phase
71 separation playing a central role in complex formation and β-catenin phosphorylation. Disruption
72 of Axin polymerization impairs LLPS formation (Bernkopf, Bruckner et al., 2019, Lach, Qiu et al.,
73 2022), promoting Wnt signaling, while β-catenin itself undergoes phase separation via
74 intrinsically disordered regions (IDRs), accumulating at super-enhancers to activate Wnt target
75 genes (Zamudio, Dall'Agnese et al., 2019).
76
77 Our analysis of the IQGAP3 interactome provides an important resource for understanding the
78 role of IQGAP3 in integrating signals from extensive protein networks in cancer. IQGAP3 functions
79 as a scaffolding platform, supporting other scaffold proteins in coordinating complex signaling
80 flux from multiple pathways. In this study, we identified Axin1 and CK1α as novel IQGAP3
81 interaction partner. We demonstrated that IQGAP3 promotes Wnt signaling by stabilizing β-
82 catenin. Mechanistically, IQGAP3 reduces Axin1-CK1α interaction, thereby inhibiting β-catenin
83 phosphorylation on Ser45 and leading to its accumulation. This global increase in β-catenin
84 subsequently promotes the expression of pro-proliferation and survival genes. Finally, we
85 identified an IQGAP3-Wnt feedback loop that sustains Wnt signaling.

86 **RESULTS**

87 **Proximity proteomics reveal IQGAP3 interaction with Cdc42, Anillin and with centrosome- and**
88 **septin-complex proteins**

89 Since both IQGAP3 and Wnt signaling play crucial roles in the maintenance of gastric stem cells
90 and carcinogenesis, we sought to understand the dynamics of IQGAP3 within the Wnt signal
91 transduction network. Given the frequent overexpression of IQGAP3 in various cancer types, we
92 utilized an IQGAP3 overexpression system to study its role in cancer progression. HEK293 cells
93 were chosen for their intact Wnt signaling cascade (i.e., no mutations in Wnt signaling
94 components) (Li, Ng et al., 2012), Wnt-responsiveness (Tuupanen, Turunen et al., 2009) and low
95 basal expression of IQGAP3. We mapped the proximal interactome of IQGAP3 in living cells using
96 the enzyme-catalyzed proximity labeling method, TurboID (Branon, Bosch et al., 2018) with and
97 without Wnt3a stimulation. To induce Wnt signaling, HEK293 Tet-On cells were treated with L-
98 Wnt3a cells (CRL-2647) conditioned media supplemented with rhWnt3a (100 ng/ml) or L-cells
99 (CRL-2648) conditioned media (control) for 4 hours (Fig. 1A). To ensure that the TurboID tag did
100 not compromise the expression, function, and localization of IQGAP3, we validated the construct
101 in three ways: expression was confirmed through immunoblot analysis using both anti-HA-tag
102 and anti-IQGAP3 antibodies (Fig. S1A), function was evaluated through anti-HA-tag
103 immunoprecipitation and probing for Anillin, an established IQGAP3 interacting partner (Adachi
104 et al., 2014) (Fig. S1B), and localization was assessed by immunofluorescence staining with anti-
105 HA antibody (Fig. S1C).

106 Prior to analysis of TurboID-IQGAP3 by label-free quantitative mass spectrometry, protein
107 expression and biotinylation levels were validated (Fig. S2A and B). 169 and 197 high-confidence
108 IQGAP3 proximity partners were identified in the L-cells conditioned media (-Wnt3a) (Fig. S2C)
109 and L-Wnt3a conditioned media (+Wnt3a) (Fig.S2D), respectively (Fold-change ≥ 4, p value ≤
110 0.01), henceforth referred to as -Wnt3a and +Wnt3a treated cells. Amongst these, 100 proximity
111 partners were found in both -Wnt3a and +Wnt3a treated cells (Fig 1B).

112 To systematically study the interactome profile changes brought about by Wnt3a treatment, we
113 identified shared proximity partners present before and after Wnt3a treatment, exclusive

114 proximity partners before and after Wnt3a treatment, and performed gene ontology analysis to
115 further characterize their compartmentalization, biological and molecular functions.

116 Consistent with published literature, we observed established interacting partners of IQGAP3,
117 such as Anillin (Adachi et al., 2014) and Cdc42 (Wang et al., 2007) in both interactomes (Fig. 1C).
118 Interestingly, topological analysis of these established partners showed high degree (*k*) within
119 the protein-protein interaction network, indicating their role as hub proteins i.e. proteins that
120 are engaged in essential interactions (Barabasi, Gulbahce et al., 2011, Fox, Hescott et al., 2011,
121 Stelzl, Worm et al., 2005). PCM1, a marker for centriolar satellites (Hori & Toda, 2017) was also
122 identified as a strongly enriched proximity partner of IQGAP3 based on its high rank and degree
123 within the interactomes (Fig. S1C and D).

124 Several complexes were also identified in both interactomes including Septin, CCR4-NOT, HAUS,
125 and myosin complexes. Gene ontology for biological process, molecular function and cellular
126 compartment indicates that the shared proximity partners of -Wnt3a and +Wnt3a treated cells
127 are enriched for Actin Filament organization, Actin binding and Cytoskeleton, in congruence with
128 its role as a regulator of actin cytoskeleton organization (Brandt & Grosse, 2007).

129

130 **Wnt3a treatment promotes IQGAP3 localization to non-membrane organelles and cell**
131 **junctions.**

132 To gain insight into the changes to IQGAP3 proximity partners upon Wnt3a treatment, we
133 compared the proximity partners that were exclusively enriched in the -Wnt3a and +Wnt3a
134 treated cells. Exclusive proximity partners of IQGAP3 in -Wnt3a treated cells (n=69) revealed
135 proteins involved in Wnt signaling; Axin1, APC, PPP2R1A and MACF1 (Fig 2A). Interestingly, all
136 four proteins are scaffold proteins. The presence of IQGAP3 within the proximity of the
137 destruction complex proteins, Axin1 and APC, indicates that it may play a role in Wnt-off
138 condition. In addition, we again observed proteins involved in the CCR4-NOT and HAUS complex,
139 which are known to be involved in mRNA metabolism (Denis & Chen, 2003) and
140 centrosome/spindle integrity (Lawo, Bashkurov et al., 2009), respectively. Lastly, proximity
141 partners found within P-bodies (i.e. dynamic non-membrane bound cytoplasmic structures) such

142 as TOB1, EIF4ENIF1/4E-T, and TNRC6C, may suggest a role for IQGAP3 in the control of translation
143 and mRNA degradation (Decker & Parker, 2012).

144 Meanwhile, exclusive proximity partners of IQGAP3 in +Wnt3a treated cells (n=97) revealed
145 increased in IQGAP3 proximity with cell junction proteins, ESCRT complex, proteins involved in
146 cell division and the centrosome. Notably, we observed the loss of IQGAP3 proximity to Axin1,
147 APC, and MACF1, along with an increased association with β-catenin and enrichment of proteins
148 present in the cell junction, such as Paxillin, Zyxin, and Moesin (Fig. 2B).

149 Next, we compared the Gene ontology for Biological Process enriched in the -Wnt3a and +Wnt3a
150 proximity partners. We observed that -Wnt3a treated cells showed enrichment for proximity
151 partners involved in centrosome cycle, cell membrane projection, microtubule transport,
152 cytoskeleton-dependent cytokinesis, regulation of cytoskeleton and supramolecular fiber
153 organization. Meanwhile +Wnt3a treated cells showed enrichment for proximity partners
154 involved in actin cytoskeleton organization, non-membrane bounded organelle-, organelle- and
155 cell projection-assembly (Fig. 2C).

156 Comparison of the Gene ontology for Cellular Component revealed that -Wnt3a treated cells
157 enriches proximity partners localized to the microtubule cytoskeleton, ruffle, cytoplasm, and
158 centriole. Whereas +Wnt3a treated cells showed enrichment of proximity partners localized to
159 the supramolecular fiber, cell-cell junction, lamellipodium, podosome and actin-based cell
160 projection. Taken together, it appears that IQGAP3 responds to Wnt signaling by first associating
161 with the destruction complex under Wnt-off conditions, and later translocating to the cell
162 junction and actin-based cell projections upon stimulation with Wnt3a.

163 **IQGAP3 undergoes phase separation**

164 To visualize changes in IQGAP3 localization within cells, we generated HeLa Tet-On cells stably
165 expressing doxycycline-inducible EGFP-empty (control) or EGFP-IQGAP3 (Fig. 3A). HeLa cells were
166 chosen because they are frequently used in imaging studies. Their large, flat morphology makes
167 them ideal for high-resolution microscopy, as it facilitates the clear visualization of cellular
168 structures, which is critical for protein localization studies.

169 Timelapse experiments revealed the formation of IQGAP3 puncta in both the cytoplasm and
170 nucleus (Fig. 3B and 3C). Furthermore, treatment of EGFP-IQGAP3 cells with Wnt3a resulted in
171 an increased localization of IQGAP3 to the cell junctions, cell projections, and cytoplasmic puncta
172 formation (Fig. 3C). Despite the differences in the cell lines used, these observations were
173 consistent with the interactome data. Next, we treated the cells with 1% 1,6-hexanediol (1,6-
174 HD), an aliphatic alcohol known to disrupt weak hydrophobic interactions and disassemble LLPS-
175 dependent macromolecular condensates with minimal cytotoxicity (Alberti, Gladfelter et al.,
176 2019). As a negative control, the cells were treated with 1% 2,5-Hexanediol (2,5-HD). To track the
177 disruption of the puncta, we performed timelapse imaging before and after 1,6-HD and 2,5-HD
178 treatments. We observed that while treatment with 1,6-HD disrupted EGFP-IQGAP3 condensates,
179 treatment with 2,5-HD did not (Fig. 3D). We next examined whether IQGAP3 puncta display
180 features distinctive of liquid-like condensates. A key feature of liquid-like condensates is their
181 internal dynamical reorganization and fast exchange kinetics (Hyman, Weber et al., 2014), which
182 can be assessed by measuring the rate of fluorescence recovery after photobleaching (FRAP). We
183 studied the dynamics of EGFP-IQGAP3 condensates by FRAP and observed that EGFP-IQGAP3
184 displayed dynamic condensate formation distinctive of liquid-like condensates capable of both
185 recovery after bleaching (half time of recovery, $\tau_{1/2}$ = 30.87s) and fusion with other condensates
186 (Fig. 3E and F).

187 **IQGAP3 co-localizes within Axin1 puncta in the cytosol.**

188 Both IQGAP1 and IQGAP3 have been implicated to be involved in Wnt signaling (Carmon et al.,
189 2014). To compare the localization of IQGAP1 and IQGAP3, we overexpressed full length IQGAP1
190 and IQGAP3 fused to mCherry2 in HeLa cells (Fig. 4B and 4C), and as control mcherry2-empty (Fig.
191 4A). We counted 50 cells that showed mCherry2-IQGAP1 or mCherry2-IQGAP3 expression and
192 categorized them based on the distribution of the IQGAP proteins i.e. when the highest intensity
193 of IQGAP expression is in the membrane, the cell is counted as Mem>Cyto, vice versa (Fig. 4D).
194 We observed that IQGAP1 is predominantly localized to the membrane (Fig. 4B) whereas IQGAP3
195 is localized both in the cytoplasm and nucleus (Fig 4C).

196 Axin1 is a proximity partner of IQGAP3 in the HEK293 interactome. Importantly, Axin1 is known
197 to form LLPS and its puncta formation is correlated with the activity of the β-catenin destruction

198 complex (Bernkopf et al., 2019, Nong, Kang et al., 2021, Schaefer & Peifer, 2019, Shi, Kang et al.,
199 2021). To study this phenomenon, we employed the HeLa cell line which is commonly used to
200 model biomolecular condensate formation *in vivo* (Muzzopappa, Hummert et al., 2022, Poudyal,
201 Patel et al., 2023, Shakya, Park et al., 2020). As controls, we expressed mCherry2-empty with
202 EGFP-empty (Fig. 4F-H) and mCherry2-empty with EGFP-Axin1 (Fig. 4I-K). Ectopic expression of
203 EGFP-Axin1 with mCherry2-IQGAP1 (Fig. 4L-N) or mCherry2-IQGAP3 (Fig. 4O-Q) revealed only the
204 colocalization of IQGAP3 within Axin1 puncta. Furthermore, exogenous co-immunoprecipitation
205 of IQGAP1 and IQGAP3 revealed that only IQGAP3 binds Axin1 (Fig. S3A and B). Taken together,
206 the differences in their subcellular distribution may explain the differential binding of IQGAP1
207 and IQGAP3 to Axin1. Therefore, although both paralogs have been linked to Wnt signaling
208 (Carmon et al., 2014), they likely contribute to distinct aspects of the Wnt signaling cascade.

209 **IQGAP3 expression reduces Axin1-CK1α interaction.**

210 Next, we confirm the endogenous interaction between IQGAP3 and the destruction complex.
211 Endogenous immunoprecipitation of IQGAP3 from HEK293 lysate revealed endogenous IQGAP3
212 interaction with Axin1, β-catenin, CK1α and PCM1 (Fig. 5A). IQGAP3 interaction with Axin1, β-
213 catenin, and CK1α confirms its presence within the destruction complex. IQGAP3 however did
214 not directly interact with other components of the destruction complex; GSK3β and PP2Aα.
215 Similarly, exogenous co-immunoprecipitation experiments involving IQGAP3 with either Axin1,
216 CK1α, GSK3β, PP2Ac, or β-catenin revealed that only Axin1 and CK1α binds to IQGAP3 (Fig. S3B-
217 F), thus indicating the specificity of the interaction.

218 To study the dynamics of IQGAP3-Axin1 interaction, we performed a time-course Wnt3a
219 treatment and performed immunoprecipitation using Axin1 antibody in HEK293T cells
220 overexpressing Myc-IQGAP3 (Fig. 5B). We note that IQGAP3-Axin1 complex formation decreases
221 at 4 hours post Wnt3a treatment due to less Axin1 precipitating as a result of Axin1 degradation
222 that occurs at 4 hour post Wnt3a treatment as others have found (Li et al., 2012). This
223 observation explained the loss of Axin1 from the interactome following Wnt3a treatment (Fig.
224 2B).

225 As expected, Wnt3a treatment showed increased Axin1-β-catenin complex formation with the
226 duration of stimulation (Li et al., 2012). Similarly, immunoprecipitation using IQGAP3 antibody

227 (Fig. 5C) showed increased IQGAP3-β-catenin complex formation with the duration of Wnt3a
228 treatment consistent with the observation that β-catenin interaction is gained in the IQGAP3
229 interactome following Wnt3a treatment (Fig. 2B).

230 To characterize the Axin1-IQGAP3 interaction, we mapped the binding domains and found that
231 IQGAP3 binds to the region between the β-catenin binding domain and the DIX domain (i.e., the
232 CK1α/PP2A binding site) of Axin1 (Fig. 5D) via its IQ and RGCT domains (Fig. S3G-I). Given that
233 IQGAP3 can bind to both CK1α and the CK1α/PP2A binding site within Axin1, we hypothesized
234 that it might disrupt the Axin1-CK1α interaction. Indeed, increased expression of IQGAP3 in
235 HEK293T cells reduced the presence of CK1α in both exogenous Axin1 (Fig. 5E) and endogenous
236 Axin1 (Fig. 5F) precipitates, confirming that IQGAP3 overexpression reduces the Axin1-CK1α
237 interaction. Although we observed that IQGAP3 interacts with Axin1, potentially blocking the
238 Axin1-CK1α interaction, we cannot rule out the possibility that overexpressed IQGAP3 also
239 sequesters CK1α away from Axin1, thereby simultaneously reducing the Axin1-CK1α interaction.

240 **IQGAP3 promotes β-catenin activity through its CC and IQ domains.**

241 We next examined the effect of IQGAP3 overexpression on Wnt signaling. Considering that β-
242 catenin is necessary for Wnt activation and that Axin1 is a critical component of β-catenin
243 destruction complex, we hypothesized that IQGAP3 interferes with β-catenin destruction by
244 reducing the Axin1-CK1α interaction. To test this, we assessed the effects of IQGAP3 depletion
245 and overexpression on exogenous β-catenin in HEK293T cells. Since free excess β-catenin is
246 rapidly phosphorylated by the destruction complex and marked for degradation (Valenta,
247 Hausmann et al., 2012), we used exogenous β-catenin expression to determine whether changes
248 in IQGAP3 could affect this process (Goentoro & Kirschner, 2009).

249 To measure β-catenin activity we perform TOPFlash assay by co-expressing β-catenin with either
250 Axin1 or an increasing amount of IQGAP3. We observed that β-catenin co-expression with Axin1
251 drastically reduced β-catenin activity, while co-expression with increasing amount of IQGAP3 led
252 to a significant increase in β-catenin activity (Fig. 6A). In contrast, β-catenin co-expression with
253 increasing amount of siIQGAP3 reduced β-catenin activity (Fig. 6B). Validation for siIQGAP3
254 knockdown (Fig. S4H).

255 The priming phosphorylation on Serine 45 of β-catenin is mediated by CK1α and facilitated by
256 Axin1. (Marin, Bustos et al., 2003). Therefore, disruption of Axin1-CK1α interaction will affect S45
257 phosphorylation and eventually β-catenin levels. Consistent with this, exogenous expressions of
258 IQGAP3 increased non-phosphorylated β-catenin (at Ser45) (hereafter, referred to as ABC), in
259 Wnt-off condition but decreased ABC level in Wnt-on condition (Fig. 6C). Hence, overexpressed
260 IQGAP3 may positively regulate β-catenin activity under Wnt-off conditions; however, it may
261 negatively regulate β-catenin activity under Wnt-on conditions. This dual role of IQGAP3 in Wnt
262 signaling may be explained by the interactome data, which shows that Wnt3a treatment,
263 combined with IQGAP3 overexpression, causes IQGAP3 to relocate to the cell junction with β-
264 catenin. Interestingly, we also observed that Wnt3a treatment increases IQGAP3 expression.

265 To identify the IQGAP3 domain involved in promoting β-catenin activity, we perform TOPFlash
266 assay with a series of IQGAP3 domain deletion constructs (Fig. 6D). Deletion of the Calponin
267 homology domain (ΔCHD), WW domain (ΔWW), GAP-related domain (ΔGRD), and RasGAP C-
268 terminal (ΔRGCT) promoted β-catenin activity (Fig. 6C lanes 3, 5, 7 and 8), whereas deletion of
269 the Coiled coil (ΔCC) and IQ domain (ΔIQ) failed to promote β-catenin activity (Fig. 6D lanes 4 and
270 6). We concluded that both CC and IQ domains are required for promoting β-catenin activity.

271 To gain insight into the function of these domains we amplified the cDNA encoding for the coiled
272 coil (L147 and F669) and IQ (V734 to P849) domains and cloned them into the EGFP-empty vector.
273 We then overexpressed EGFP-coiled coil (CC) and EGFP-IQ in HeLa cells. We observed that EGFP-
274 CC generated distinct puncta formation (Fig. 6G). Similarly, when we studied the dynamics of
275 EGFP-CC condensates using FRAP, we found that EGFP-CC exhibited even higher dynamics in
276 condensate formation after bleaching with a half time of recovery at $\tau_{1/2}$=7.42s compared to
277 EGFP-IQGAP3 at $\tau_{1/2}$=30.87s (Fig. 6G-I). In addition, IQGAP3 deletion of various domains (Fig. S4A-
278 G) showed loss of puncta formation when cell was transfected with the mCherry2-IQGAP3ΔCC
279 construct (Fig. S4C).

280 Meanwhile, cells overexpressed with EGFP-IQ displayed mainly nuclear localization of the
281 peptide (Fig. 6I-K). To confirm that IQ domain is sufficient and necessary for nuclear localization
282 we overexpressed IQGAP3 with an IQ domain deletion (mCherry2-IQGAP3ΔIQ). We observed
283 that IQ deletion abolished any presence of nuclear IQGAP3 (Fig.6L-N) compared to the deletions
284 of other domains (Fig.S4A-G), therefore, the IQ domain within IQGAP3 may harbor a nuclear

285 localization signal (NLS) required for its nuclear localization. To predict the presence of an NLS,
286 we performed an *in silico* analysis of the IQGAP3 protein sequence using NLStradamus (Nguyen
287 Ba, Pogoutse et al., 2009) and cNLS Mapper (Kosugi, Hasebe et al., 2009). Neither analysis
288 predicted an NLS within IQGAP3. Therefore, we hypothesized that the IQ domain might instead
289 bind to a protein with an NLS, mediating IQGAP3's nuclear translocation—essentially 'hitchhiking'
290 into the nucleus. Taken together, the CC and IQ domains mediate IQGAP3 phase separation and
291 nuclear localization, respectively. Therefore, it appears that the ability of IQGAP3 to promote β-
292 catenin activity is dependent on its ability to phase separate and translocate to the nucleus.

293 **IQGAP3 overexpression increases β-catenin levels in MKN28 cells.**

294 To determine IQGAP3-low and-high expressing gastric cancer cell lines, we screened several
295 gastric cancer cell lines for the expression of IQGAP3 (Fig. 7A). NUGC3 and AGS cells showed high
296 IQGAP3 expression, whereas MKN28 cells showed low IQGAP3 expression, hence, the latter was
297 deemed a suitable candidate to study the effect of IQGAP3 overexpression in gastric cancer cells.
298 We generated MKN28 cells stably overexpressing doxycycline-inducible 3×Flag-IQGAP3 and upon
299 treatment with doxycycline showed increased β-catenin levels (Fig. 7B).

300 Next, we generated MKN28 cells stably overexpressing doxycycline-inducible 3×HA-TurboID-
301 IQGAP3 for RNA-seq analysis and proximity ligation. Induction of fusion protein expressions and
302 biotinylating activities were analyzed by immunoblot (Fig. S5A and S5B). The RNA-seq analysis
303 from IQGAP3 overexpressing cells revealed an enrichment for several signaling pathways, G2/M,
304 TGF-β, NOTCH, and Wnt/β-catenin in the GSEA data (Fig. 7C). Similarly, the gene ontology analysis
305 of the Biological Process (GO) revealed enrichment in the Wnt signaling pathway (Fig. 7D), the
306 Molecular Function (GO) showed enrichment in Wnt-protein and beta-catenin binding (Fig. 7E),
307 and the KEGG pathway analysis indicated enrichment in Hippo, Notch and Wnt signaling
308 pathways (Fig. 7F). For the full list of GSEA rankings from RNA-sequencing analysis see Fig. S5C.
309 We also validated the MKN28 cells for IQGAP3-Axin1 interaction and changes in Wnt target genes
310 (*Axin2* and *TCF7*) expression upon IQGAP3 overexpression via immunoprecipitation and RT-qPCR,
311 respectively (Fig. S5E and F).

312 Next, we performed the biotinylation ligation of IQGAP3 proximity partners in MKN28 cells. Prior
313 to analysis of TurboID-IQGAP3 by label-free quantitative mass spectrometry, protein expression

314 and biotinylation levels were validated (Fig. S5A and B). 232 high-confidence IQGAP3 proximity
315 partners were identified (Fold-change ⩾ 2, p value ⩽ 0.05) (Fig. 7G). Proximity ligation of
316 IQGAP3 within MKN28 cells revealed Axin1 as a proximity partner of IQGAP3. The presence of
317 IQGAP3 in proximity to Axin1 in both HEK293 and MKN28 cells strongly suggests its involvement
318 in the destruction complex. Moreover, proteins involved in cell junction, septin complex, and
319 centrosome are also found in the MKN28 interactome.

320 Surprisingly, we observed a greater number of nuclear proteins (nucleoplasm proteins) as
321 IQGAP3 proximity partners in MKN28 cells compared to HEK293 cells. Among these nuclear
322 proteins, seven (CTR9, PRPF3, ASCC2, NSRP1, HECTD1, ZNF217, and DHX36) were associated with
323 nuclear speckles formation. Similarly, when analyzing endogenous IQGAP3 localization in non-
324 transformed cell lines (HEK293T and HFE145) and transformed gastric cell lines (MKN1, MKN28,
325 HS746T, and NUGC3), we found that in transformed cells, IQGAP3 staining exhibited a more
326 punctate morphology and showed a higher nuclear presence compared to non-transformed cells
327 (Fig. S6A-C).

328

329 **IQGAP3 knock-out decreases β-catenin levels in NUGC3 and AGS cells.**

330 The canonical Wnt pathway is best known for its regulation of cell proliferation (Jung & Park,
331 2020). We next ascertained how IQGAP3 status affects Wnt-driven proliferative potential, we
332 performed CRISPR-mediated IQGAP3 knock-out in two gastric cancer cell lines: the *TP53* mutant
333 NUGC3 and the constitutively active Tcf transcriptional activity (CTTA) AGS cell line (Caca, Kolligs
334 et al., 1999). As screened previously, both cell lines exhibit high IQGAP3 expression (Fig. 7A),
335 making them suitable candidates for CRISPR-mediated knock-out.

336 IQGAP3-KO NUGC3 cells showed reduced total β-catenin levels (Fig. 8A) and decreased
337 expression of Wnt target genes (*CCND1* and *MYC*) (Fig. 8B) compared to NUGC3 wild-type cells.
338 Moreover, both cell proliferation (Fig. 8C) and clonogenic growth (Fig. 8D and E) were also
339 impaired.

340 Relevant to Wnt signaling, AGS harbor mutations for the following proteins; *CTNNB1* (G34E) (Caca
341 et al., 1999) and *CDH1 (*G579fs) (Caldeira, Figueiredo et al., 2015). These mutations result in the

342 accumulation of β-catenin and loss of E-cadherin expression, respectively. Loss of IQGAP3
343 impaired cell proliferation and clonogenic growth in the AGS gastric cancer cell line (Fig. 8H-J).
344 Importantly, AGS IQGAP3 knock-out (IQ3KO) displayed significant loss of β-catenin relative to the
345 AGS parental counterpart (Fig. 8F). Concomitantly, the expression of Wnt target genes involved
346 in promoting proliferation and cell-cycle re-entry, *CCND1* and *Myc* (Niehrs & Acebron, 2012,
347 Nusse, 2008, van de Wetering, Sancho et al., 2002) were also reduced in AGS IQ3KO cells (Fig.
348 8G).

349 In line with our findings, the relationship between IQGAP3 expression and β-catenin levels has
350 also been previously observed, whereby the loss of IQGAP3 expression via siRNA-mediated
351 knockdown in pancreatic cancer cell lines BxPC-3 and SW1990 have been shown to reduce β-
352 catenin expression (Xu, Xu et al., 2016). Hence, our observation that the loss of IQGAP3 reduces
353 β-catenin expression in gastric cancer cells may also apply to other cancer types.

354

355 **IQGAP3 is a target of Wnt signaling, sustains Wnt signaling via positive feedback loop.**

356 Wnt activity in epithelial stem cells are tightly regulated. Wnt-signaling levels below a specific
357 threshold can be lethal due to the rapid turnover rate of the epithelium, as observed in mouse
358 models of Tcf4 conditional knock-out (van Es, Haegebarth et al., 2012) or DKK overexpression
359 (Kuhnert, Davis et al., 2004). Conversely, excessively high Wnt-signaling resulted in the
360 overproduction of crypts, the formation of adenomas, and the development of cancer (Polakis,
361 2012). To maintain stringent control, the pathway incorporates various molecular checkpoints
362 and feedback loops, where pathway components (e.g. AXIN2 (Leung, Kolligs et al., 2002), DKK1
363 (Niida, Hiroko et al., 2004), SFRP1 (Caldwell, Jones et al., 2006), WIF1 (He, Reguart et al., 2005),
364 CD44 (Schmitt, Metzger et al., 2015), and NKD1 (Van Raay, Coffey et al., 2007)) play distinct
365 regulatory roles.

366

367 To assess whether IQGAP3 is involved in the Wnt feedback loop, we treated HEK293T cells with
368 Wnt3a conditioned media and analyzed IQGAP3 transcript and protein expression. As expected,
369 RT-qPCR revealed increased expression of known Wnt targets, including AXIN2, CCND1, MYC,
370 LEF1, TCF7, and TCF7L2 (also known as TCF4), following Wnt3a conditioned media treatment.

371 Interestingly, we also observed a Wnt3a-associated increase in IQGAP3 transcript levels (Fig. 9A).
372 Supporting this, a time-course analysis of Wnt3a conditioned media treatment in HEK293T cells
373 showed elevated IQGAP3 expression over time (Fig. 9B). Additionally, probing for IQGAP3
374 expression in L cells and L-Wnt3a cells revealed higher IQGAP3 levels in L-Wnt3a cells compared
375 to L cells (Fig. S6D). Together, these findings strongly suggest that IQGAP3 is a Wnt target gene.
376
377 We next investigated how Wnt signaling regulates *IQGAP3* transcription. The Genome browser
378 revealed multiple canonical TCF4 binding motifs (A/T-A/T-C-A-A-A-G or C-T-T-T-G-A/T-A/T) (van
379 de Wetering & Clevers, 1992) within the *IQGAP3* promoter (*IQGAP3*P). The promoter region of
380 *IQGAP3* spanning 4320bp (-3000 to +1320bp of TSS), a series of *IQGAP3*P 5'-truncations, and
381 *Axin2* promoter *(Axin2*P) spanning 1730bp (-581 to +1149bp of TSS) were cloned into the pGL3-
382 basic firefly luciferase reporter vector. We observed that both the full length *IQGAP3*P (-3000 to
383 +1320 of TSS) and *Axin2*P responded to Wnt3a treatment, while the truncated *IQGAP3*P
384 constructs did not (Fig. 9C). Thus, we hypothesized that a Wnt Responsive Element (WRE) might
385 reside within -3000 to -2000bp of the TSS. Indeed, a truncation comprising the smaller fragment
386 of -3000 to -2000bp (Site 1) displayed strong luciferase activity upon Wnt3a-CM treatment,
387 similar to *Axin2*P, whereas negative control Site 2 (+335 to +1265 of the TSS) did not (Fig. 9D).
388 Within Site1 we identified two potential WREs located within -2815 to -2808bp and -2810 to -
389 2803bp of the TSS, harboring the motifs CTTTGAA and CTTTGTA, respectively. Next, we mutated
390 the motifs: CTTTG<u>AA</u> to CTTTG<u>GC</u> (Site1aM) and CTTTG<u>TA</u> to CTTTG<u>GC</u> (Site1bM) and observed
391 that both Site1a and Site1b are necessary for Wnt3a-mediated upregulation of IQGAP3
392 transcription (Fig.9E). Lastly, we validated whether inhibition of Wnt signaling affects IQGAP3
393 expression by treating cells with XAV939, a Tankyrase (TNKS) inhibitor, that functions to stabilize
394 Axin1 (Huang, Mishina et al., 2009). Time-course treatment with XAV939 increases Axin1
395 expression while decreasing both β-catenin and IQGAP3 expression (Fig 9F). Taken together, our
396 findings confirm that IQGAP3 is a Wnt target.
397

398 **DISCUSSION**

399 Scaffold protein IQGAP3 is upregulated in most, if not all, cancer cells and has been shown to be
400 required for proliferation (Nojima et al., 2008). Identifying the IQGAP3 interactome in cancer cells
401 is thus a critical step to develop anti-IQGAP3 therapeutics in cancer. Traditional
402 immunoprecipitation/mass spectrometry techniques may miss transient, but crucial interactions
403 in the IQGAP3 scaffold function. Here, we utilize Proximity ligation labelling to systemically
404 characterize the molecular interactions and mechanisms underlying the IQGAP3 scaffold function
405 in cancer.

406 We identified large networks of IQGAP3 interacting proteins in the cell cycle as well as oncogenic
407 pathways. Based on our interactome data, IQGAP3 is associated with different protein complexes
408 located at various locations of the cell and phases of the cell cycle. We observed that IQGAP3
409 proximity partners were enriched for proteins found in non-membrane bounded organelle or
410 phase separated microenvironment. By forming interactions with other phase-separated scaffold
411 proteins, IQGAP3 could penetrate the specialized microenvironments of various biochemical
412 reactions and thus regulate these reactions.

413 In this study, we have uncovered a previously unknown function of IQGAP3. IQGAP3 expression
414 disrupts Axin1-CK1α interaction, either by blocking CK1α binding to Axin1, sequestering CK1α
415 away from Axin1, or both, thereby inhibiting β-catenin phosphorylation and promoting its
416 stabilization (Fig 10). Notably, we identified that the coiled-coil (CC) domain of IQGAP3 is essential
417 for its phase separation, while the IQ domain is necessary for its nuclear localization. Both
418 functions are critical for IQGAP3 to enhance β-catenin activity. This dependence on the coiled-
419 coil domain to phase separate resembles proteins such as, Amot (Wang, Choi et al., 2022, Wells,
420 Fawcett et al., 2006), KIBRA (Wang et al., 2022), SLMAP (Wang et al., 2022), TAZ (Lu, Wu et al.,
421 2020), YAP (Mao, Liu et al., 2023), liprin-α (Liang, Jin et al., 2021), LINE-1 ORF (Newton, Naik et
422 al., 2021), and RNA-Binding Proteins (RBPs) (Ford & Fioriti, 2020). In addition, the IQ domain
423 potentially mediates IQGAP3 nuclear localization through hitchhiking on proteins harboring an
424 NLS. Elucidating this mechanism could provide insight into the role of IQGAP3 in the nucleus.

425 In addition, we observed that Wnt3a treatment promotes IQGAP3 expression both at the
426 transcript and protein levels. Wnt signaling is tightly regulated with multiple feedback loops,

427 where most Wnt regulators are themselves Wnt target genes (Zhong & Virshup, 2020). Similarly,
428 IQGAP3 is both a regulator and target of Wnt signaling. This Wnt-associated function of IQGAP3
429 supports previous findings that implicate IQGAP3 in promotion of cancer proliferation and stem
430 cell regeneration. Therefore, targeting IQGAP3 during early stages of cancer could potentially
431 help mitigate both the growth and spread of cancers.

432 **MATERIALS AND METHODS**

433

434 **Cell culture, transfection and conditioned media**

435 HEK293T (CRL-3216), L-Cells (CRL-2648), and L-Wnt3a cells (CRL-2647) were from ATCC. HEK293
436 Tet-On® 3G Cell Line #631182 was from Takara bio. Immortalized human normal gastric epithelial
437 cells (HFE145) were obtained from Dr. Hassan Ashktorab and Dr. Duane Smoot. Both HEK293 and
438 HEK293T cells were cultured in Dulbecco's modified Eagle's medium (DMEM) while the gastric
439 cancer cell lines, AGS, MKN1, MKN28, HFE145 and NUGC3 cells were cultured in RPMI-1640, both
440 growth media were supplemented with 10% fetal bovine serum (FBS) and 1% Penicillin-
441 Streptomycin solution. The Dox-inducible 3×HA-TurboID-empty and 3×HA-TurboID-IQGAP3
442 expressing cells were generated by transfection of pRetroX-3×HA-TurboID-empty or pRetroX-
443 3×HA-TurboID-IQGAP3 in the HEK293-Tet-On and MKN28-Tet-On cells, thereafter, stable
444 population were selected with 1.0 µg/ml Puromycin.

445 All Dox-inducible TurboID stable expressing cells were cultured and maintained in DMEM
446 supplemented with 10% fetal bovine serum (FBS), 0.5 µg/ml Puromycin (Gibco), 1 µg/ml
447 Doxycycline (Sigma), 200 µg/ml Geneticin (Gibco). Transfections were carried out using
448 Lipofectamine 2000 (Thermofisher) according to the manufacturer's instructions. CRISPR knock-
449 out cells were cultured and maintained in RPMI supplemented with 10% fetal bovine serum (FBS),
450 and 0.5 µg/ml Puromycin. Conditioned media from L-cells and L-Wnt3a cells were harvested 72-
451 96 hours after cell seeding and filtered through 0.45 µm syringe filter and stored in -80°C. All
452 Wnt3a conditioned media were supplemented with 100 ng/ml rhWnt3a #5036-WN
453 (RnDSystems).

454 All cell lines were verified for authenticity prior to use and screened for mycoplasma
455 contamination every three months using the LookOut® Mycoplasma qPCR Detection Kit (Sigma
456 Aldrich).

457

458 **Antibodies and Plasmids**

459 Antibodies specific for the following proteins were used at the indicated dilutions for Immunoblot:
460 α-Tubulin 11224-1-AP (1:10,000, Proteintech®); IQGAP3 #25930-1-AP, mCherry #26765-1-AP (all
461 1:1000, Proteintech®); Flag M2 #F1804 (1:1000, Sigma); Axin1 #2087, β-catenin #8480, Non-
462 phospho (Active) β-Catenin (Ser45) #19807, Non-phospho (Active) β-Catenin (Ser33/37/Thr41)
463 #8814, Myc-Tag #2276, HA-Tag #3724 (rabbit) & #2367 (mouse), GSK-3β #12456 (rabbit) & #9832
464 (mouse), PP2A C #2038 (all 1:1000, Cell Signaling). Streptavidin-HRP #ab7403 (1:40,000, Abcam);
465 IQGAP1 #ab86064 (1:1000, Abcam), CK1α Antibody (H-7): sc-74582 (1:250, Santa Cruz).

466 Antibodies specific for the following proteins were used at the indicated dilutions for
467 immunoprecipitation: Axin1 #2087 (1:100, Cell Signaling), Myc-Tag (9B11) #2276 (1:100, Cell
468 Signaling). Anti-Flag® M2 #F1804 (1:100 Sigma), IQGAP3 (H00128239PW2) #89-301-822 (1:100,
469 Abnova).

470 The following plasmid was obtained from Vectorbuilder:

471 pCMV-EGFP-IQGAP3

472 The following plasmids were obtained from Addgene:

473 3xHA-TurboID pRetrox (from Kyle Roux, #155203), pGL3-OT and pGL3-OF (from Bert Vogelstein,
474 #16558 & #16559), Flag-Axin1 (from Mariann Bienz, #109370), β-catenin-Flag (from Eric Fearon,
475 #16828), LentiCRISPRv2 (from Feng Zheng, #52961), pMD2.G and psPAX2 (from Didier Trono
476 #12259 and #12260), mCherry2-C1 (from Michael Davidson, #54563), pcDNA3-EGFP-empty
477 (Doug Golenbock, #13031), pcDNA3-GSK3β-HA (from Jim Woodgett, # 14753), pLC-Flag-
478 CSNK1A1 WT-Puro (from Eva Gottwein #123319)

479

480 **Molecular cloning**

481 Cloning was performed using either In-Fusion HD Cloning Kits (Takara) via Ligation Independent
482 Cloning (LIC) or Restriction cloning using enzymes purchased from New England Biolabs (NEB).

483 Full-length IQGAP3 coding sequence was cloned from pCMV-IQGAP3-GFP and inserted into
484 3xHA-TurboID pRetrox, pcDNA3-Flag-empty, pcDNA3-Myc-empty, and mCherry2-C1. Full-length

485 Axin1 coding sequence was cloned from Flag-Axin1 and inserted into pcDNA3-EGFP-empty and
486 pcDNA3-HA-empty. Full-length β-catenin coding sequence was cloned from β-catenin-Flag and
487 inserted into pcDNA3-HA-empty. Full-length CK1α coding sequence was cloned from pLC-Flag-
488 CSNK1A1 WT-Puro and inserted into pcDNA3-HA-empty.

489 cDNA expressing EGFP-CC was amplified from the pCMV-EGFP-IQGAP3 vector using the following
490 primers: EcoRI-CC-For, TAAGCAGAATTCCTCTTCCTCTTCCGGCTGGG and XhoI-CC-Rev,
491 TGCTTACTCGAGGAAAGCTGTGTCTGCTGG generating a 1593 bp primer product that was later
492 cloned into an EGFP-vector backbone. Similarly, EGFP-IQ was amplified from pCMV-EGFP-
493 IQGAP3 vector using the following primers: EcoRI-IQ-For,
494 TAAGCAGAATTCGTTATCCAGCTCCAGGCCCG and XhoI-IQ-Rev,
495 TGCTTACTCGAGCTAAGGGTGGGGTGCATGCAC generating a 375 bp primer product that was later
496 cloned into an EGFP-vector backbone.

497

498 **Promoter cloning**

499 Promoter sequences of *AXIN2* and *IQGAP3* were obtained from Ensembl. *IQGAP3* promoter
500 (*IQGAP3P*): A region spanning 4320bp located on chr1: 156,571,285-156,575,604 (GRCh38/hg38)
501 or chr1:156,541,077-156,545,396 (GRCh37/hg19) and *AXIN2* promoter (*AXIN2P*): A region
502 spanning 1730bp located on chr17: 65,560,500-65,562,229 (GRCh38/hg38) or chr17:63,556,618-
503 63,558,347 (GRCh37/hg19). Both promoter sequences were PCR amplified using genomic DNA
504 isolated from HEK293T cells with KAPA HiFi PCR Kit. Primer-BLAST was used to verify the
505 specificity of primer design. In-Fusion HD Cloning Kits (Takara) were used in Ligation Independent
506 Cloning (LIC) of PCR product into pGL3 basic vector. Primer sequences excluding homology
507 sequences (added for LIC) are as follows, for *IQGAP3P* forward primer: 5'-
508 ACCTATAGATGTAACTTGTCCAAG-'3 and reverse primer: 5'-GTAAGAAAATAAACTCAGAGAGCTT-3',
509 for *AXIN2P* forward primer: 5'-CACTCAGGCCTATACTGGCG-3' and reverse primer: 5'-
510 CACGCCGACTCACATCCATA-3'. All promoter plasmid constructs were co-transfected with pSV-β-
511 Galactosidase (internal control) into HEK293T cells with and without Wnt3a-CM treatment to
512 validate the putative Wnt responsive element (WRE) within the promoter region.

513

514 **gRNA design and plasmids**

515 The sgRNA sequence including PAM region targeting exon 5 of *IQGAP3* was determined using IDT
516 (sg.idtdna.com/site/order/designtool/index/CRISPR_SEQUENCE) as follows; 5'-
517 TGGATGCAGTAGACTACCCG GGG-3'. While sgRNA targeting exon 17 of *IQGAP3* was determined
518 using CRISPR Design Tool (www.genscript.com/CRISPR-gRNA-constructs.html) as follows; 5'-
519 GTCGGGAACTACCCCTCGAA GGG-3'. sgRNA oligos were cloned into LentiCRISPRv2 plasmid
520 (Addgene #52961) at BsmBI restriction sites (Sanjana, Shalem et al., 2014).

521

522 **Lentiviral vector construction and transduction**

523 Lentiviral vectors were produced by co-transfecting HEK293T cells with the transfer plasmid
524 sgRNA-Cas9-expressing lentiCRISPRv2, the packaging plasmid pMD2.G and psPAX2 using
525 Lipofectamine 2000 transfection reagent. Briefly, for each sgRNA, a plate of 10-cm plate of 60%
526 confluent 293T cells was transfected with 10 µg of the transfer plasmid, 5µg of pMD2.G, 7.5µg of
527 psPAX2, and 40 ul of Lipofectamine 2000 (Life Technologies). After 24 hours, the media was
528 replaced with fresh media. After 48 hours, viral supernatants were collected and centrifuged at
529 3,000 rpm at 4 °C for 5 min to pellet cell debris. The supernatant was filtered through a 0.45 µm
530 low protein binding membrane (Millipore) and used immediately after supplementing with
531 7µg/ml of polybrene or stored in -80°C. Successful knock-out colonies were selected with
532 Puromycin treatment, 1 µg /ml.

533

534 **Immunoblot**

535 Cells were lysed with RIPA lysis buffer (ThermoSci) supplemented with Protease inhibitor cocktail
536 (Roche) and Halt™ Phosphatase Inhibitor Cocktail (Thermo Scientific™). For all unless specified,
537 20 µg of total protein from each sample were subjected to 7.5% or 10% SDS polyacrylamide gel
538 electrophoresis (PAGE) and electrophoretic transfer onto 0.2 µm polyvinylidene difluoride (PVDF)
539 membrane (Bio-Rad) at 30 V, 100 mA, 4 °C overnight. The transfer buffer (Towbin) comprises
540 25 mM Tris, 192 mM glycine, 20% (v/v) methanol, pH 8.3. Membranes were incubated with
541 primary antibodies in either 0.5% BSA or skimmed milk in TBST (Tris Buffered Saline + 0.1% (v/v)

542 Tween 20) overnight, following which were washed 3 times with TBST and incubated with
543 secondary antibody conjugated with HRP (1:5000) in 0.5% BSA or skimmed milk in TBST for 1
544 hour at room temperature. Membranes were then washed 3 times with TBST. Antibody detection
545 was performed using Radiance plus chemiluminescent substrate (azure biosystems). Antibody
546 reactions detection was imaged using ImageQuant LAS 500 (GE Healthcare). When re-probing
547 with a different primary antibody, membranes were stripped using Mild stripping buffer pH 2.2
548 (1.5% (w/v) Glycine, 1% (w/v) SDS, and 1% Tween 20) in room temperature for 10 minutes and
549 thereafter washed with TBS for 10 minutes twice and with TBST for 10 minutes twice. All
550 immunoblotting were performed thrice, only best represented images were used. Uncropped
551 images of all immunoblots can be found in the supplementary image file.

552

553 **Immunofluorescence staining**

554 Cells were fixed with 4% paraformaldehyde for 30 minutes and washed with PBS three times for
555 5 minutes each. Cells were then permeabilized with PBS containing 0.1% Triton X-100 for 10
556 minutes. Permeabilized cells were then incubated in blocking buffer (0.5% BSA/0.1% Triton X-
557 100) for 1 hour, and following that with the appropriate primary antibody diluted in antibody
558 dilution buffer (0.5% BSA/0.3% Triton X-100) overnight in 4˚C. After three washes with PBS for 5
559 minutes each, cells were incubated with Alexa Fluor 488- or 594-conjugated secondary
560 antibodies (1:100 dilution) for 1 hour. Cells were then washed with PBS three times for 5 minutes
561 each and mounted with DAPI. Fluorescence was observed under Zeiss LSM 880 Airy Scan.

562

563 **Live Cell Imaging**

564 HeLa Tet-On cells stably expressing Doxycycline inducible EGFP-empty and EGFP-IQGAP3 were
565 seeded onto a 35 mm cell imaging dish with a glass bottom (Matsunami). Cells were induced with
566 Doxycycline 24-48 hours prior to live imaging.

567

568 **Fluorescence recovery after photobleaching (FRAP)**

569 HeLa cells grown on Glass Bottom Culture Dishes (Matsunami Glass) were transfected with 2 µg
570 per well of GFP–CC and analyzed through quantitative FRAP studies 24h after transfection. FRAP
571 experiments were performed using a Zeiss LSM880 confocal microscope. The fluorescence signal
572 was bleached using 100% of maximum laser power of the 488-nm laser with 150 interactions for
573 ~2.5 s. Relative recovery was normalized to the initial (before bleaching) fluorescence intensity
574 for each bleached condensate and then used to calculate mean and SD of the recovery time. To
575 compare the post-bleach recovery 5 pre-bleach images were captured.

576 For the treatment of 1,6-hexanediol (1,6-HD), culture media was replaced with 5% 1,6 HD
577 prepared in DMEM culture media, which was replaced with fresh culture media to monitor the
578 recovery after 1,6 HD treatment. Apart from the bleached region, fluorescence intensity mean
579 was also recorded for non-bleached and background. Raw FRAP data was further analyzed using
580 easyFRAP online analysis tool (Koulouras et al., 2018). All acquired images were processed and
581 analyzed in ImageJ software.

582

583 **Co-immunoprecipitation**

584 Cells were lysed with immunoprecipitation lysis buffer (IPLB) containing 25 mM Tris pH 7.5, 150
585 mM NaCl, 0.5% Triton-X, protease inhibitor cocktail (Roche) and Halt™ Phosphatase Inhibitor
586 Cocktail (Thermo Scientific™). For Flag-tagged and endogenous protein immunoprecipitation, cell
587 lysates were incubated with Protein G magnetic beads (Millipore) for 2 hours (pre-clearing). The
588 beads were removed, and primary antibody was then added to protein lysates at a concentration
589 of 1:100 and incubated overnight at 4°C. 15 µl of Protein G magnetic beads (Millipore) is then
590 added to the Protein-Antibody complex and incubated at 4°C for 2 hours. The Protein G magnetic
591 beads (Millipore) were then washed with IPLB three times and protein complex were eluted by
592 adding SDS sample buffer and boiling for 5 minutes.

593

594 **Biotin pulldowns**

595 Using the TurboID method (Branon et al., 2018), proteins in close proximity to IQGAP3 were
596 biotinylated and isolated by streptavidin-bead pulldowns. Briefly, 24 hr after Dox induction and

597 biotin supplementation (50 µM), biotinylated proteins were enriched from the protein extracts
598 with 50 µL of streptavidin-coated magnetic beads (Dynabeads™ MyOne™ Streptavidin C1,
599 Invitrogen, #65001). Beads were washed twice with RIPA lysis buffer, the lysates containing 2 mg
600 protein were then incubated with the equilibrated beads on a rotator overnight at 4 °C. The beads
601 were washed twice each with wash buffer 1 (2% SDS), wash buffer 2 (50 mM Hepes pH 7.5, 500
602 mM NaCl, 1 mM EDTA, 1% Triton-X-100, 0.5% Na-deoxycholate), wash buffer 3 (10 mM Tris pH
603 8, 250 mM LiCl, 1 mM EDTA, 0.5% NP-40, 0.5% Na-deoxycholate) and wash buffer 4 (50 mM Tris
604 pH 7.5, 50 mM NaCl, 0.1% NP-40). Biotinylated proteins were eluted by boiling the beads in 35
605 µL of 1 × Laemmli sample buffer. Eluted proteins were sent for Mass spectrometry analysis.

606

607 **Mass spectrometry analysis**

608 TurboID samples were separated on a 4-12% NuPAGE Bis-Tris precast gel (Thermo Fisher
609 Scientific) for 10 min at 170 V in 1x MOPS buffer. The gel was fixed using the Colloidal Blue
610 Staining Kit (Thermo Fisher Scientific) and processed as a single fraction. For in-gel digestion,
611 samples were destained in destaining buffer (25 mM ammonium bicarbonate; 50% ethanol),
612 reduced in 10 mM DTT for 1h at 56°C followed by alkylation with 55mM iodoacetamide (Sigma)
613 for 45 min in the dark. Tryptic digest was performed in 50 mM ammonium bicarbonate buffer
614 with 2 µg trypsin (Promega) at 37°C overnight. Peptides were desalted on StageTips and analysed
615 by nanoflow liquid chromatography on an EASY-nLC 1200 system coupled to a Q Exactive HF mass
616 spectrometer (Thermo Fisher Scientific). Peptides were separated on a C18-reversed phase
617 column (25 cm long, 75 µm inner diameter) packed in-house with ReproSil-Pur C18-AQ 1.9 µm
618 resin (Dr Maisch). The column was mounted on an Easy Flex Nano Source and temperature
619 controlled by a column oven (Sonation) at 40°C. A 105-min gradient from 2 to 40% solution B (80%
620 acetonitrile, 0.1% formic acid) at a flow of 225 nl/min was used. Spray voltage was set to 2.2 kV.
621 The Q Exactive HF was operated with a TOP20 MS/MS spectra acquisition method per MS full
622 scan. MS scans were conducted with 60,000 at a maximum injection time of 20 ms and MS/MS
623 scans with 15,000 resolution at a maximum injection time of 75 ms. The raw files were processed
624 with MaxQuant version 2.0.1.0 (HEK293) and 1.5.2.8. (MKN28) with preset standard settings for
625 label-free quantitation using the MaxLFQ algorithm. Carbamidomethylation was set as fixed
626 modification while methionine oxidation and protein N-acetylation were considered as variable

627 modifications. Search results were filtered with a false discovery rate of 0.01. Known
628 contaminants, proteins groups only identified by site, and reverse hits of the MaxQuant results
629 were removed and only proteins with LFQ intensities in four replicates of at least one condition
630 of each pair-wise comparison were kept. Missing LFQ intensities were randomly inputed from a
631 normal distribution around the lowest 5% of LFQ intensities based on the means of three
632 iterations.

633

634 **Cell Proliferation Assay**

635 Cell proliferation was determined using the TACS® XTT Cell Proliferation Assay (R&D Systems,
636 Inc.), following the manufacturer's instructions. Gastric cancer cell lines NUGC3 and AGS along
637 with their corresponding IQGAP3KOs were seeded at 1×10^3 cells/mL density in 100 µL of
638 appropriate growth medium in 96-well microplates. After incubation overnight, to allow cell
639 attachment, which was considered as 0H and analyzed, followed by analysis after time periods
640 of 24, 48, 72 and 96 hours. For analysis, 50 µL of XTT Working Solution (prepared by combining
641 XTT Reagent and XTT Activator as per kit instructions) were added to each well. Plates were
642 incubated for 6 hours at 37°C in a 5% CO_2 atmosphere. The absorbance was measured at 490 nm
643 (test wavelength) with a reference wavelength of 630-690 nm using a microplate reader. The
644 calculations are as follows: Cell Viability (%) = $(A_t / A_{0h}) \times 100$

645 Where: A_t = Absorbance of treated wells at respective time points (0, 24, 48, 72, 96 hrs) and A_{0h}
646 = Absorbance of control wells at 0h.

647

648 **Clonogenic Assay**

649 Gastric cancer cell lines NUGC3 and AGS along with their corresponding IQGAP3KOs were seeded
650 in 6-well plates at a density of 500 cells per well in 2 mL of complete growth medium and
651 incubated at 37°C in 5% CO_2. The cells were grown with necessary media change when required
652 for 7–14 days to allow colony formation. At the end of the incubation period, the medium was
653 removed, and cells were gently rinsed with PBS. Colonies were fixed and stained with a mixture
654 of 6.0% glutaraldehyde and 0.5% crystal violet for 30 minutes. The staining solution was removed,

655 and plates were rinsed in tap water and air-dried at room temperature. Colonies consisting of
656 ≥50 cells were counted manually under a light microscope. The colony-forming efficiency (CFE)
657 was calculated as: CFE (%) = Colonies formed / Cells seeded×100

658

659 **Luciferase assay**

660 5×10^4 HEK293T cells were grown per well in a 24-well plate for 24 hours, thereafter cells were
661 transfected with the appropriate plasmids: for TOPFLash (TCF wild-type (OT) or TCF mutant (OF)
662 plasmids); for promoter analysis (*IQ3P* or *Axin2P*), together with pSV-β-Galactosidase vector as
663 control vector for monitoring the transfection efficiency. Cells were grown for an additional 48-
664 hours before lysis. If Wnt3a conditioned media were used, cells were exposed to the conditioned
665 media 24-hours before lysis. Lysis was performed using 5×Passive lysis buffer (Promega, #E1910),
666 lysates were rocked in room temperature for 15 mins. Thereafter, lysates were centrifuged for
667 10 mins at 14,000 rpm to remove cell debris. Lysate supernatants used were aliquoted into white,
668 flat bottom, 96-well plate (Costar) for treatment with either Beta-Glo® (Promega, #E4720) or
669 Luciferase Assay Reagent II/LARII (Promega, #E1910) reagent.

670

671 **Real-Time Polymerase chain reaction (RT-PCR)**

672 RNA extraction was performed using RNeasy Mini Kit (Qiagen). 1 µg of Purified RNA was reverse
673 transcribed to complementary DNA (cDNA) using iScript™ Reverse Transcription Supermix (Bio-
674 Rad). cDNA was diluted 10×. RT-PCR was performed on QuantStudio™ 3 Real-Time PCR System
675 (Applied Biosystems). The 20 µl PCR reaction mixture consisted of 2 µl of cDNA, 100 nM forward
676 and reverse primers, 2× iTaq Universal SYBR Green Supermix. Cycling conditions were initial
677 denaturation at 95 °C for 5 minutes, followed by 40 cycles consisting of 95 °C for 10 seconds, 60 °C
678 for 30 seconds and 72 °C for 10 seconds.

679 The primers used for real-time RT-PCR were as follows:

Genes	**Forward (**5'-3')	**Reverse (**5'-3')
AXIN2	AGCTTACATGAGTAATGGGG	AATTCCATCTACACTGCTGTC
CCND1	TCTACACCGACAACTCCATCCG	TCTGGCATTTTGGAGAGGAGGTG

MYC	CTTCTCTCCGTCCTCGGATTCT	GAAGGTGATCCAGACTCTGACCTT
LEF1	GGTCCTCCTGGTCCCCACACAA	TCATGCTGAGGCTTCACGTGCA
TCF7	CTGACCTCTCTGGCTTCTACTC	CAGAACCTAGCATCAAGGATGGG
TCF7L2	GAATCGTCCCAGAGTGATGTCG	TGCACTCAGCTACGACCTTTGC
IQGAP3	GTTCGGCAGAAGTTTGCTGAGC	CACTCCAGGTAAATCTTCCGCTG
GAPDH	TCTTTTGCGTCGCCAGCCGA	ACCAGGCGCCCAATACGACC

680

681 **Fluorescence Intensity Analysis**

682 To determine mCherry2 intensity for localization of IQGAP1 and IQGAP3. The cross-sectional line
683 was drawn in ImageJ. Lines were fixed by the ROI manager to ensure a similar length for image
684 comparison. Lines were then analyzed using Plot Profile.

685

686 **Co-localization Analysis**

687 To determine mCherry2/EGFP co-localization, channels were split in ImageJ and the JACoP plugin
688 was used. The Pearson's Coefficient generated from 50 cells were averaged.

689

690 **General Statistical Analysis**

691 Experimental data are presented as the mean ± SD. Two-tailed Student's t tests with unequal
692 variance were performed using XLMiner Analysis ToolPak on Microsoft excel.
693 Error bars represent standard deviation. Differences were considered statistically significant
694 when p values were less than 0.05 ($^{*}p < 0.05$, $^{**}p < 0.01$, $^{***}p < 0.001$). The best represented
695 images were shown.

696

697 **Author contributions**

698 M.B.R. conceptualized the study. M.B.R. and Y.I. analyzed the data. A.H. performed XTT and
699 Clonogenic assays. D.K. and S.P. performed the mass spectrometry analysis. M.B.R. and T.Y.X.
700 performed the confocal imaging. M.B.R and B.D. performed the FRAP analysis. M.B.R. created
701 the Tet-On and CRISPR-KO cells. M.B.R. and Y.I. wrote the manuscript.

ACKNOWLEDGEMENTS

We thank Dr. Hassan Ashktorab and Dr. Duane Smoot for the Immortalized human normal gastric epithelial cells (HFE145).

This research was supported by grants from the National Research Foundation Singapore and the Singapore Ministry of Education under its Research Centers of Excellence initiative, the Singapore Ministry of Health's National Medical Research Council under its Clinician-Scientist Individual Research Grant (MOH-000933-00) and the National Medical Research Council's Open Fund Large Collaborative Grant (OFLCG18May-0023), National University of Singapore School of Medicine (NUSMed) Internal Grant Funding (NUHSRO/2019/086/ StomachStemCell and NUHSRO/2022/043/NUSMed/25/LOA) to Y.I.

CONFLICTS OF INTEREST

The authors declare that they have no competing interest.

716 **REFERENCES**

717 Adachi M, Kawasaki A, Nojima H, Nishida E, Tsukita S (2014) Involvement of IQGAP family proteins in the
718 regulation of mammalian cell cytokinesis. Genes Cells 19: 803-20
719 Alberti S, Gladfelter A, Mittag T (2019) Considerations and Challenges in Studying Liquid-Liquid Phase
720 Separation and Biomolecular Condensates. Cell 176: 419-434
721 Banani SF, Rice AM, Peeples WB, Lin Y, Jain S, Parker R, Rosen MK (2016) Compositional Control of
722 Phase-Separated Cellular Bodies. Cell 166: 651-663
723 Barabasi AL, Gulbahce N, Loscalzo J (2011) Network medicine: a network-based approach to human
724 disease. Nat Rev Genet 12: 56-68
725 Bernkopf DB, Bruckner M, Hadjihannas MV, Behrens J (2019) An aggregon in conductin/axin2 regulates
726 Wnt/beta-catenin signaling and holds potential for cancer therapy. Nat Commun 10: 4251
727 Brandt DT, Grosse R (2007) Get to grips: steering local actin dynamics with IQGAPs. EMBO Rep 8: 1019-
728 23
729 Branon TC, Bosch JA, Sanchez AD, Udeshi ND, Svinkina T, Carr SA, Feldman JL, Perrimon N, Ting AY
730 (2018) Efficient proximity labeling in living cells and organisms with TurboID. Nat Biotechnol 36: 880-887
731 Caca K, Kolligs FT, Ji X, Hayes M, Qian J, Yahanda A, Rimm DL, Costa J, Fearon ER (1999) Beta- and
732 gamma-catenin mutations, but not E-cadherin inactivation, underlie T-cell factor/lymphoid enhancer
733 factor transcriptional deregulation in gastric and pancreatic cancer. Cell Growth Differ 10: 369-76
734 Caldeira J, Figueiredo J, Bras-Pereira C, Carneiro P, Moreira AM, Pinto MT, Relvas JB, Carneiro F, Barbosa
735 M, Casares F, Janody F, Seruca R (2015) E-cadherin-defective gastric cancer cells depend on Laminin to
736 survive and invade. Hum Mol Genet 24: 5891-900
737 Caldwell GM, Jones CE, Taniere P, Warrack R, Soon Y, Matthews GM, Morton DG (2006) The Wnt
738 antagonist sFRP1 is downregulated in premalignant large bowel adenomas. Br J Cancer 94: 922-7
739 Carmon KS, Gong X, Yi J, Thomas A, Liu Q (2014) RSPO-LGR4 functions via IQGAP1 to potentiate Wnt
740 signaling. Proc Natl Acad Sci U S A 111: E1221-9
741 Decker CJ, Parker R (2012) P-bodies and stress granules: possible roles in the control of translation and
742 mRNA degradation. Cold Spring Harb Perspect Biol 4: a012286
743 Denis CL, Chen J (2003) The CCR4-NOT complex plays diverse roles in mRNA metabolism. Prog Nucleic
744 Acid Res Mol Biol 73: 221-50
745 Ford LK, Fioriti L (2020) Coiled-Coil Motifs of RNA-Binding Proteins: Dynamicity in RNA Regulation. Front
746 Cell Dev Biol 8: 607947
747 Fox AD, Hescott BJ, Blumer AC, Slonim DK (2011) Connectedness of PPI network neighborhoods
748 identifies regulatory hub proteins. Bioinformatics 27: 1135-42
749 Goentoro L, Kirschner MW (2009) Evidence that fold-change, and not absolute level, of beta-catenin
750 dictates Wnt signaling. Mol Cell 36: 872-84
751 Goh JY, Feng M, Wang W, Oguz G, Yatim S, Lee PL, Bao Y, Lim TH, Wang P, Tam WL, Kodahl AR, Lyng MB,
752 Sarma S, Lin SY, Lezhava A, Yap YS, Lim AST, Hoon DSB, Ditzel HJ, Lee SC et al. (2017) Chromosome
753 1q21.3 amplification is a trackable biomarker and actionable target for breast cancer recurrence. Nat
754 Med 23: 1319-1330
755 He B, Reguart N, You L, Mazieres J, Xu Z, Lee AY, Mikami I, McCormick F, Jablons DM (2005) Blockade of
756 Wnt-1 signaling induces apoptosis in human colorectal cancer cells containing downstream mutations.
757 Oncogene 24: 3054-8
758 Hori A, Toda T (2017) Regulation of centriolar satellite integrity and its physiology. Cell Mol Life Sci 74:
759 213-229
760 Hu X, Wu X, Berry K, Zhao C, Xin D, Ogurek S, Liu X, Zhang L, Luo Z, Sakabe M, Trubicka J, Lastowska M,
761 Szulzewsky F, Holland EC, Lee L, Hu M, Xin M, Lu QR (2023) Nuclear condensates of YAP fusion proteins
762 alter transcription to drive ependymoma tumourigenesis. Nat Cell Biol 25: 323-336
763 Huang SM, Mishina YM, Liu S, Cheung A, Stegmeier F, Michaud GA, Charlat O, Wiellette E, Zhang Y,
764 Wiessner S, Hild M, Shi X, Wilson CJ, Mickanin C, Myer V, Fazal A, Tomlinson R, Serluca F, Shao W, Cheng
765 H et al. (2009) Tankyrase inhibition stabilizes axin and antagonizes Wnt signalling. Nature 461: 614-20

766 Hyman AA, Weber CA, Julicher F (2014) Liquid-liquid phase separation in biology. Annu Rev Cell Dev Biol
767 30: 39-58
768 Jung YS, Park JI (2020) Wnt signaling in cancer: therapeutic targeting of Wnt signaling beyond beta-
769 catenin and the destruction complex. Exp Mol Med 52: 183-191
770 Kosugi S, Hasebe M, Tomita M, Yanagawa H (2009) Systematic identification of cell cycle-dependent
771 yeast nucleocytoplasmic shuttling proteins by prediction of composite motifs. Proc Natl Acad Sci U S A
772 106: 10171-6
773 Kuhnert F, Davis CR, Wang HT, Chu P, Lee M, Yuan J, Nusse R, Kuo CJ (2004) Essential requirement for
774 Wnt signaling in proliferation of adult small intestine and colon revealed by adenoviral expression of
775 Dickkopf-1. Proc Natl Acad Sci U S A 101: 266-71
776 Lach RS, Qiu C, Kajbaf EZ, Baxter N, Han D, Wang A, Lock H, Chirikian O, Pruitt B, Wilson MZ (2022)
777 Nucleation of the destruction complex on the centrosome accelerates degradation of beta-catenin and
778 regulates Wnt signal transmission. Proc Natl Acad Sci U S A 119: e2204688119
779 Lawo S, Bashkurov M, Mullin M, Ferreria MG, Kittler R, Habermann B, Tagliaferro A, Poser I, Hutchins JR,
780 Hegemann B, Pinchev D, Buchholz F, Peters JM, Hyman AA, Gingras AC, Pelletier L (2009) HAUS, the 8-
781 subunit human Augmin complex, regulates centrosome and spindle integrity. Curr Biol 19: 816-26
782 Leung JY, Kolligs FT, Wu R, Zhai Y, Kuick R, Hanash S, Cho KR, Fearon ER (2002) Activation of AXIN2
783 expression by beta-catenin-T cell factor. A feedback repressor pathway regulating Wnt signaling. J Biol
784 Chem 277: 21657-65
785 Li VS, Ng SS, Boersema PJ, Low TY, Karthaus WR, Gerlach JP, Mohammed S, Heck AJ, Maurice MM,
786 Mahmoudi T, Clevers H (2012) Wnt signaling through inhibition of beta-catenin degradation in an intact
787 Axin1 complex. Cell 149: 1245-56
788 Liang M, Jin G, Xie X, Zhang W, Li K, Niu F, Yu C, Wei Z (2021) Oligomerized liprin-alpha promotes phase
789 separation of ELKS for compartmentalization of presynaptic active zone proteins. Cell Rep 34: 108901
790 Lin M, Liu Y, Ding X, Ke Q, Shi J, Ma Z, Gu H, Wang H, Zhang C, Yang C, Fang Z, Zhou L, Ye M (2019) E2F1
791 transactivates IQGAP3 and promotes proliferation of hepatocellular carcinoma cells through IQGAP3-
792 mediated PKC-alpha activation. Am J Cancer Res 9: 285-299
793 Lu Y, Wu T, Gutman O, Lu H, Zhou Q, Henis YI, Luo K (2020) Phase separation of TAZ compartmentalizes
794 the transcription machinery to promote gene expression. Nat Cell Biol 22: 453-464
795 Mao S, Liu Q, Wu H, Zhu J, Xie Y, Ma J, Zhen N, Pan Q (2023) Phase separation of YAP mediated by
796 coiled-coil domain promotes hepatoblastoma proliferation via activation of transcription. J
797 Gastroenterol Hepatol
798 Marin O, Bustos VH, Cesaro L, Meggio F, Pagano MA, Antonelli M, Allende CC, Pinna LA, Allende JE
799 (2003) A noncanonical sequence phosphorylated by casein kinase 1 in beta-catenin may play a role in
800 casein kinase 1 targeting of important signaling proteins. Proc Natl Acad Sci U S A 100: 10193-200
801 Matsuo J, Douchi D, Myint K, Mon NN, Yamamura A, Kohu K, Heng DL, Chen S, Mawan NA, Nuttonmanit
802 N, Li Y, Srivastava S, Ho SWT, Lee NYS, Lee HK, Adachi M, Tamura A, Chen J, Yang H, Teh M et al. (2020)
803 Iqgap3-Ras axis drives stem cell proliferation in the stomach corpus during homoeostasis and repair. Gut
804 Matsuo J, Douchi D, Myint K, Mon NN, Yamamura A, Kohu K, Heng DL, Chen S, Mawan NA, Nuttonmanit
805 N, Li Y, Srivastava S, Ho SWT, Lee NYS, Lee HK, Adachi M, Tamura A, Chen J, Yang H, Teh M et al. (2021)
806 Iqgap3-Ras axis drives stem cell proliferation in the stomach corpus during homoeostasis and repair. Gut
807 70: 1833-1846
808 Mehta S, Zhang J (2022) Liquid-liquid phase separation drives cellular function and dysfunction in
809 cancer. Nat Rev Cancer 22: 239-252
810 Meng F, Yu Z, Zhang D, Chen S, Guan H, Zhou R, Wu Q, Zhang Q, Liu S, Venkat Ramani MK, Yang B, Ba
811 XQ, Zhang J, Huang J, Bai X, Qin J, Feng XH, Ouyang S, Zhang YJ, Liang T et al. (2021) Induced phase
812 separation of mutant NF2 imprisons the cGAS-STING machinery to abrogate antitumor immunity. Mol
813 Cell 81: 4147-4164 e7

814 Monteleon CL, McNeal A, Duperret EK, Oh SJ, Schapira E, Ridky TW (2015) IQGAP1 and IQGAP3 Serve
815 Individually Essential Roles in Normal Epidermal Homeostasis and Tumor Progression. J Invest Dermatol
816 135: 2258-2265
817 Muzzopappa F, Hummert J, Anfossi M, Tashev SA, Herten DP, Erdel F (2022) Detecting and quantifying
818 liquid-liquid phase separation in living cells by model-free calibrated half-bleaching. Nat Commun 13:
819 7787
820 Myint K, Chuang LSH, Teh YX, Mawan NA, Shi EJ, Mok MMH, Nuttonmanit N, Matsuo J, Li Y, Yang H,
821 Okabe A, Kaneda A, Osato M, So JB, Yong WP, Tan P, Yeoh KG, Ito Y (2022) Oncofetal protein IGF2BP1
822 regulates IQGAP3 expression to maintain stem cell potential in cancer. iScience 25: 105194
823 Nesterov SV, Ilyinsky NS, Uversky VN (2021) Liquid-liquid phase separation as a common organizing
824 principle of intracellular space and biomembranes providing dynamic adaptive responses. Biochim
825 Biophys Acta Mol Cell Res 1868: 119102
826 Newton JC, Naik MT, Li GY, Murphy EL, Fawzi NL, Sedivy JM, Jogl G (2021) Phase separation of the LINE-1
827 ORF1 protein is mediated by the N-terminus and coiled-coil domain. Biophys J 120: 2181-2191
828 Nguyen Ba AN, Pogoutse A, Provart N, Moses AM (2009) NLStradamus: a simple Hidden Markov Model
829 for nuclear localization signal prediction. BMC Bioinformatics 10: 202
830 Niehrs C, Acebron SP (2012) Mitotic and mitogenic Wnt signalling. EMBO J 31: 2705-13
831 Niida A, Hiroko T, Kasai M, Furukawa Y, Nakamura Y, Suzuki Y, Sugano S, Akiyama T (2004) DKK1, a
832 negative regulator of Wnt signaling, is a target of the beta-catenin/TCF pathway. Oncogene 23: 8520-6
833 Nojima H, Adachi M, Matsui T, Okawa K, Tsukita S, Tsukita S (2008) IQGAP3 regulates cell proliferation
834 through the Ras/ERK signalling cascade. Nat Cell Biol 10: 971-8
835 Nong J, Kang K, Shi Q, Zhu X, Tao Q, Chen YG (2021) Phase separation of Axin organizes the beta-catenin
836 destruction complex. J Cell Biol 220
837 Nusse R (2008) Wnt signaling and stem cell control. Cell Res 18: 523-7
838 Polakis P (2012) Wnt signaling in cancer. Cold Spring Harb Perspect Biol 4
839 Poudyal M, Patel K, Gadhe L, Sawner AS, Kadu P, Datta D, Mukherjee S, Ray S, Navalkar A, Maiti S,
840 Chatterjee D, Devi J, Bera R, Gahlot N, Joseph J, Padinhateeri R, Maji SK (2023) Intermolecular
841 interactions underlie protein/peptide phase separation irrespective of sequence and structure at
842 crowded milieu. Nat Commun 14: 6199
843 Ramakrishnan AB, Cadigan KM (2017) Wnt target genes and where to find them. F1000Res 6: 746
844 Sanchez-Laorden B, Viros A, Marais R (2013) Mind the IQGAP. Cancer Cell 23: 715-7
845 Sanjana NE, Shalem O, Zhang F (2014) Improved vectors and genome-wide libraries for CRISPR
846 screening. Nat Methods 11: 783-784
847 Schaefer KN, Peifer M (2019) Wnt/Beta-Catenin Signaling Regulation and a Role for Biomolecular
848 Condensates. Dev Cell 48: 429-444
849 Schmitt M, Metzger M, Gradl D, Davidson G, Orian-Rousseau V (2015) CD44 functions in Wnt signaling
850 by regulating LRP6 localization and activation. Cell Death Differ 22: 677-89
851 Shakya A, Park S, Rana N, King JT (2020) Liquid-Liquid Phase Separation of Histone Proteins in Cells: Role
852 in Chromatin Organization. Biophys J 118: 753-764
853 Shi Q, Kang K, Chen YG (2021) Liquid-liquid phase separation drives the beta-catenin destruction
854 complex formation. Bioessays 43: e2100138
855 Stelzl U, Worm U, Lalowski M, Haenig C, Brembeck FH, Goehler H, Stroedicke M, Zenkner M, Schoenherr
856 A, Koeppen S, Timm J, Mintzlaff S, Abraham C, Bock N, Kietzmann S, Goedde A, Toksoz E, Droege A,
857 Krobitsch S, Korn B et al. (2005) A human protein-protein interaction network: a resource for annotating
858 the proteome. Cell 122: 957-68
859 Tong X, Tang R, Xu J, Wang W, Zhao Y, Yu X, Shi S (2022) Liquid-liquid phase separation in tumor biology.
860 Signal Transduct Target Ther 7: 221
861 Tuupanen S, Turunen M, Lehtonen R, Hallikas O, Vanharanta S, Kivioja T, Bjorklund M, Wei G, Yan J,
862 Niittymaki I, Mecklin JP, Jarvinen H, Ristimaki A, Di-Bernardo M, East P, Carvajal-Carmona L, Houlston RS,

863 Tomlinson I, Palin K, Ukkonen E et al. (2009) The common colorectal cancer predisposition SNP
864 rs6983267 at chromosome 8q24 confers potential to enhanced Wnt signaling. Nat Genet 41: 885-90
865 Valenta T, Hausmann G, Basler K (2012) The many faces and functions of beta-catenin. EMBO J 31: 2714-
866 36
867 van de Wetering M, Clevers H (1992) Sequence-specific interaction of the HMG box proteins TCF-1 and
868 SRY occurs within the minor groove of a Watson-Crick double helix. EMBO J 11: 3039-44
869 van de Wetering M, Sancho E, Verweij C, de Lau W, Oving I, Hurlstone A, van der Horn K, Batlle E,
870 Coudreuse D, Haramis AP, Tjon-Pon-Fong M, Moerer P, van den Born M, Soete G, Pals S, Eilers M,
871 Medema R, Clevers H (2002) The beta-catenin/TCF-4 complex imposes a crypt progenitor phenotype on
872 colorectal cancer cells. Cell 111: 241-50
873 van Es JH, Haegebarth A, Kujala P, Itzkovitz S, Koo BK, Boj SF, Korving J, van den Born M, van
874 Oudenaarden A, Robine S, Clevers H (2012) A critical role for the Wnt effector Tcf4 in adult intestinal
875 homeostatic self-renewal. Mol Cell Biol 32: 1918-27
876 Van Raay TJ, Coffey RJ, Solnica-Krezel L (2007) Zebrafish Naked1 and Naked2 antagonize both canonical
877 and non-canonical Wnt signaling. Dev Biol 309: 151-68
878 Vazquez-Mena O, Medina-Martinez I, Juarez-Torres E, Barron V, Espinosa A, Villegas-Sepulveda N,
879 Gomez-Laguna L, Nieto-Martinez K, Orozco L, Roman-Basaure E, Munoz Cortez S, Borges Ibanez M,
880 Venegas-Vega C, Guardado-Estrada M, Rangel-Lopez A, Kofman S, Berumen J (2012) Amplified genes
881 may be overexpressed, unchanged, or downregulated in cervical cancer cell lines. PLoS One 7: e32667
882 Wang L, Choi K, Su T, Li B, Wu X, Zhang R, Driskill JH, Li H, Lei H, Guo P, Chen EH, Zheng Y, Pan D (2022)
883 Multiphase coalescence mediates Hippo pathway activation. Cell 185: 4376-4393 e18
884 Wang S, Watanabe T, Noritake J, Fukata M, Yoshimura T, Itoh N, Harada T, Nakagawa M, Matsuura Y,
885 Arimura N, Kaibuchi K (2007) IQGAP3, a novel effector of Rac1 and Cdc42, regulates neurite outgrowth. J
886 Cell Sci 120: 567-77
887 Wells CD, Fawcett JP, Traweger A, Yamanaka Y, Goudreault M, Elder K, Kulkarni S, Gish G, Virag C, Lim C,
888 Colwill K, Starostine A, Metalnikov P, Pawson T (2006) A Rich1/Amot complex regulates the Cdc42
889 GTPase and apical-polarity proteins in epithelial cells. Cell 125: 535-48
890 Xu W, Xu B, Yao Y, Yu X, Cao H, Zhang J, Liu J, Sheng H (2016) Overexpression and biological function of
891 IQGAP3 in human pancreatic cancer. Am J Transl Res 8: 5421-5432
892 Yang Y, Zhao W, Xu QW, Wang XS, Zhang Y, Zhang J (2014) IQGAP3 promotes EGFR-ERK signaling and the
893 growth and metastasis of lung cancer cells. PLoS One 9: e97578
894 Zamudio AV, Dall'Agnese A, Henninger JE, Manteiga JC, Afeyan LK, Hannett NM, Coffey EL, Li CH, Oksuz
895 O, Sabari BR, Boija A, Klein IA, Hawken SW, Spille JH, Decker TM, Cisse, II, Abraham BJ, Lee TI, Taatjes DJ,
896 Schuijers J et al. (2019) Mediator Condensates Localize Signaling Factors to Key Cell Identity Genes. Mol
897 Cell 76: 753-766 e6
898 Zhong Z, Virshup DM (2020) Wnt Signaling and Drug Resistance in Cancer. Mol Pharmacol 97: 72-89

899

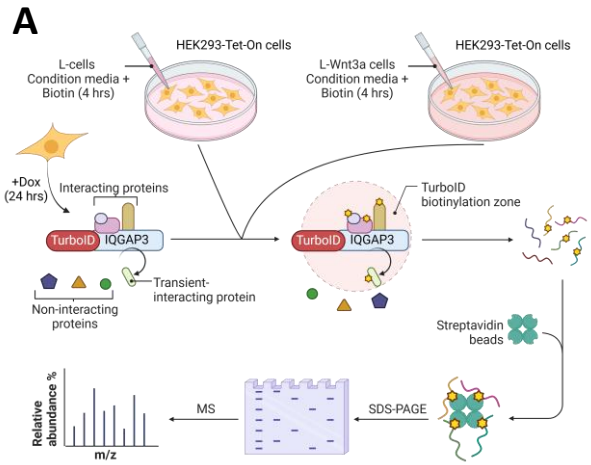

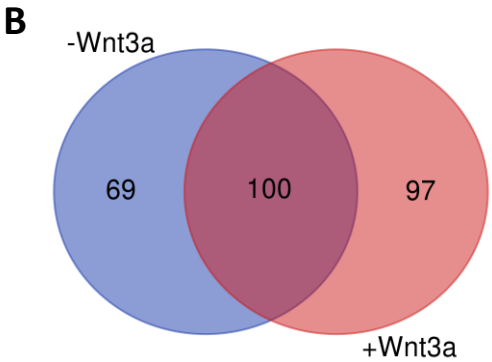

Fold change ≥ 4, p-value ≤ 0.01

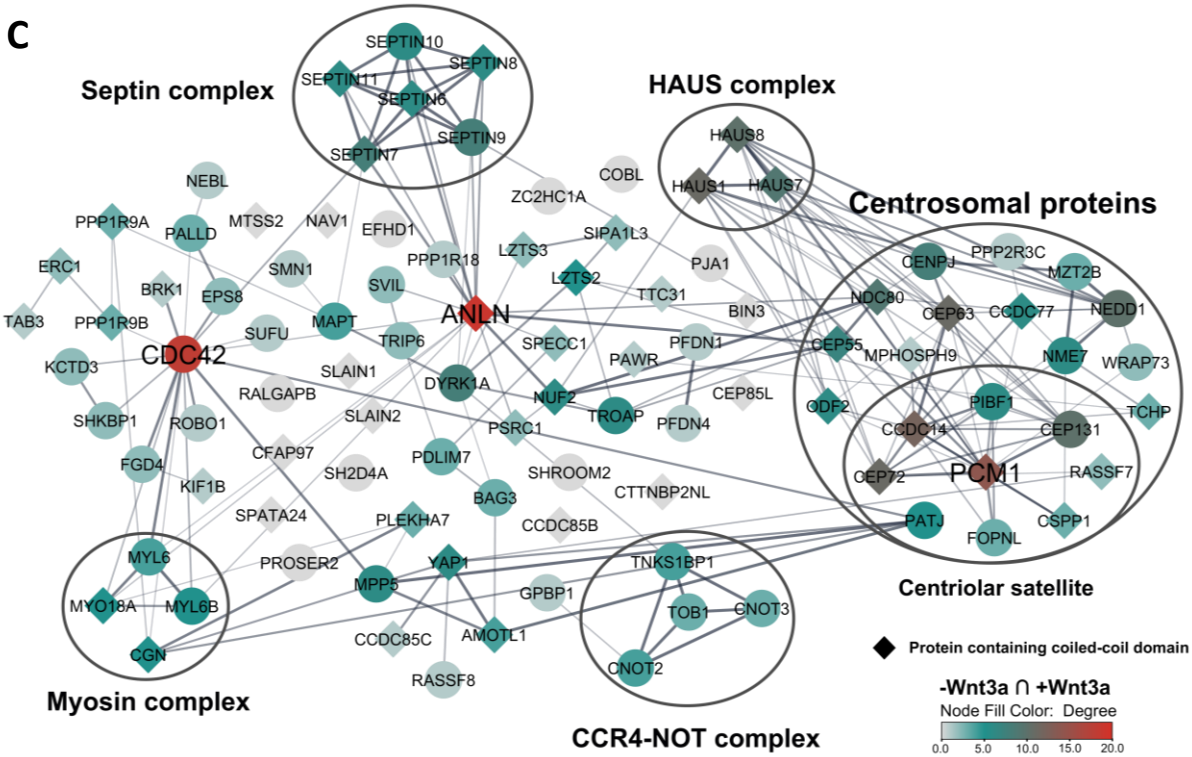

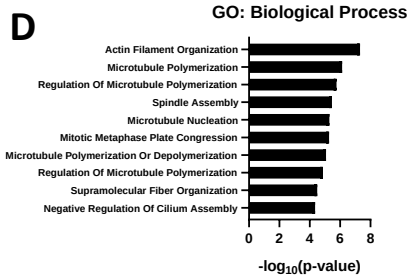

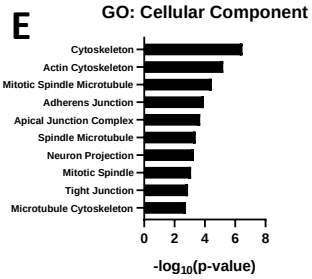

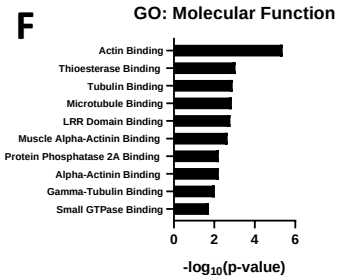

Fig. 1. Proximity proteomics reveal IQGAP3 interaction with Cdc42, Anillin and with centrosome- and septin-complexes. (A) Workflow for proximity-dependent identification of IQGAP3-associated proteins in HEK293 cells treated with either L-cells condition media (-Wnt3a) or L-Wnt3a cells condition media (+Wnt3a) treatment for 4 hours, Created with BioRender.com. (B) Venn diagram of biotinylated proteins detected in HEK293 cells treated with L-cells condition media (-Wnt3a) and L-Wnt3a cells condition media (+Wnt3a) (Fold change ≥ 4, p-value ≤ 0.01). (C) Interactome of -Wnt3a ∩ +Wnt3a (Fold change ≥ 4, p-value ≤ 0.01), node color denote degree distribution, Created with Cytoscape. (D) Gene ontology: Biological Process of shared proximity partners in -Wnt3a and +Wnt3a treated cells. (E) Gene ontology: Molecular function of shared proximity partners in -Wnt3a and +Wnt3a treated cells. (F) Gene ontology: Cellular compartment of shared proximity partners in -Wnt3a and +Wnt3a treated cells.

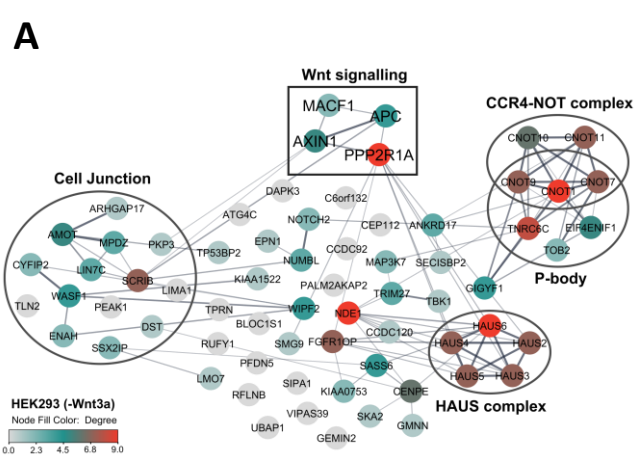
A
Wnt signalling
MACF1
APC
AXIN1
PPP2R1A
CCR4-NOT complex
CNOT10
CNOT11
CNOT9
CNOT1
CNOT7
TNRC6C
EIF4ENIF1
TOB2
P-body
Cell Junction
ARHGAP17
AMOT
MPDZ
PKP3
CYFIP2
LIN7C
SCRIB
WASF1
LIMA1
TLN2
PEAK1
ENAH
DST
SSX2IP
DAPK3
ATG4C
C6orf132
NOTCH2
EPN1
TP53BP2
CEP112
ANKRD17
CCDC92
NUMBL
MAP3K7
SECISBP2
KIAA1522
PALM2AKAP2
TRIM27
TBK1
GIGYF1
TPRN
WIPF2
NDE1
BLOC1S1
CCDC120
RUFY1
SMG9
FGFR10P
HAUS6
HAUS4
HAUS2
HAUS5
HAUS3
PFDN5
SASS6
LMO7
SIPA1
KIAA0753
CENPE
RFLNB
VIPAS39
SKA2
GMNN
UBAP1
GEMIN2
HAUS complex
HEK293 (-Wnt3a)
Node Fill Color: Degree
0.0 2.3 4.5 6.8 9.0

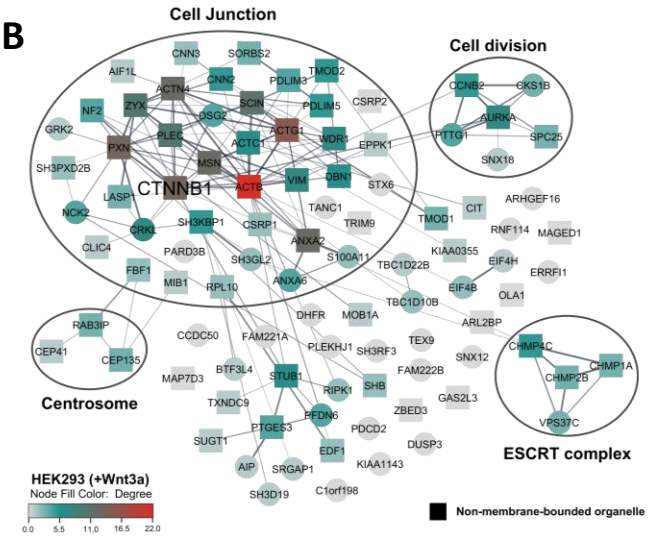
B
Cell Junction
CNN3
SORBS2
AIF1L
TMOD2
CNN2
PDLIM3
ACTN4
ZYX
SCIN
PDLIM5
CSRP2
NF2
DSG2
GRK2
PLEC
ACTG2
PXN
ACTC1
VDR
EPPK1
MSN
SH3PXD2B
CTNNB1
ACTB
VIM
DBN1
STX6
LASP1
TANC1
NCK2
CRKL
SH3KBP1
CSRP1
TRIM9
CLIC4
PARD3B
ANXA2
S100A11
FBF1
SH3GL2
MIB1
RPL10
ANXA6
DHFR
MOB1A
RAB3IP
CEP41
CEP135
CCDC50
FAM221A
PLEKHJ1
SH3RF3
MAP7D3
BTF3L4
STUB1
RIPK1
SHB
TXNDC9
PFDN6
PTGES3
PDCD2
SUGT1
EDF1
AIP
SRGAP1
SH3D19
C1orf198
Centrosome
Cell division
CCNB2
CKS1B
AURKA
FTTG1
SPC25
SNX18
ARHGEF16
CIT
TMOD1
RNF114
MAGED1
KIAA0355
EIF4H
ERRFI1
TBC1D22B
EIF4B
OLA1
TBC1D10B
ARL2BP
TEX9
SNX12
FAM222B
GAS2L3
ZBED3
DUSP3
KIAA1143
CHMP4C
CHMP1A
CHMP2B
VPS37C
ESCRT complex
HEK293 (+Wnt3a)
Node Fill Color: Degree
0.0 5.5 11.0 16.5 22.0
Non-membrane-bounded organelle

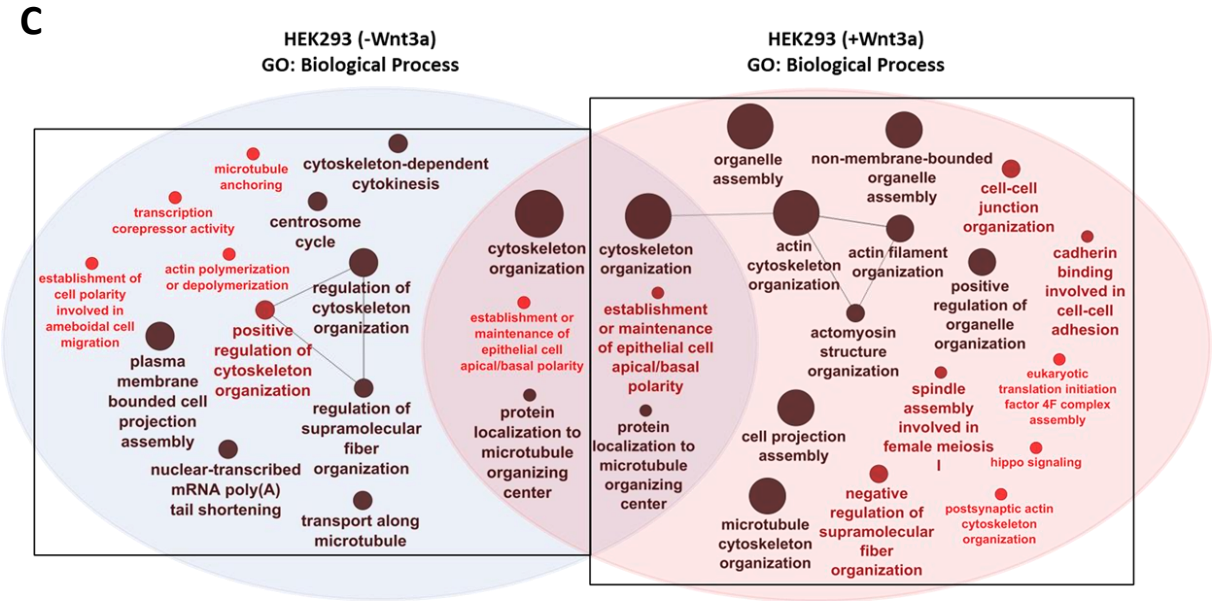
C
HEK293 (-Wnt3a)
GO: Biological Process
microtubule anchoring
cytoskeleton-dependent cytokinesis
transcription corepressor activity
centrosome cycle
establishment of cell polarity involved in ameboidal cell migration
actin polymerization or depolymerization
regulation of cytoskeleton organization
positive regulation of cytoskeleton organization
plasma membrane bounded cell projection assembly
regulation of supramolecular fiber organization
nuclear-transcribed mRNA poly(A) tail shortening
transport along microtubule
HEK293 (+Wnt3a)
GO: Biological Process
cytoskeleton organization
establishment or maintenance of epithelial cell apical/basal polarity
protein localization to microtubule organizing center
organelle assembly
non-membrane-bounded organelle assembly
cell-cell junction organization
actin cytoskeleton organization
actin filament organization
cadherin binding involved in cell-cell adhesion
positive regulation of organelle organization
actomyosin structure organization
spindle assembly involved in female meiosis I
eukaryotic translation initiation factor 4F complex assembly
cell projection assembly
hippo signaling
negative regulation of supramolecular fiber organization
postsynaptic actin cytoskeleton organization
microtubule cytoskeleton organization

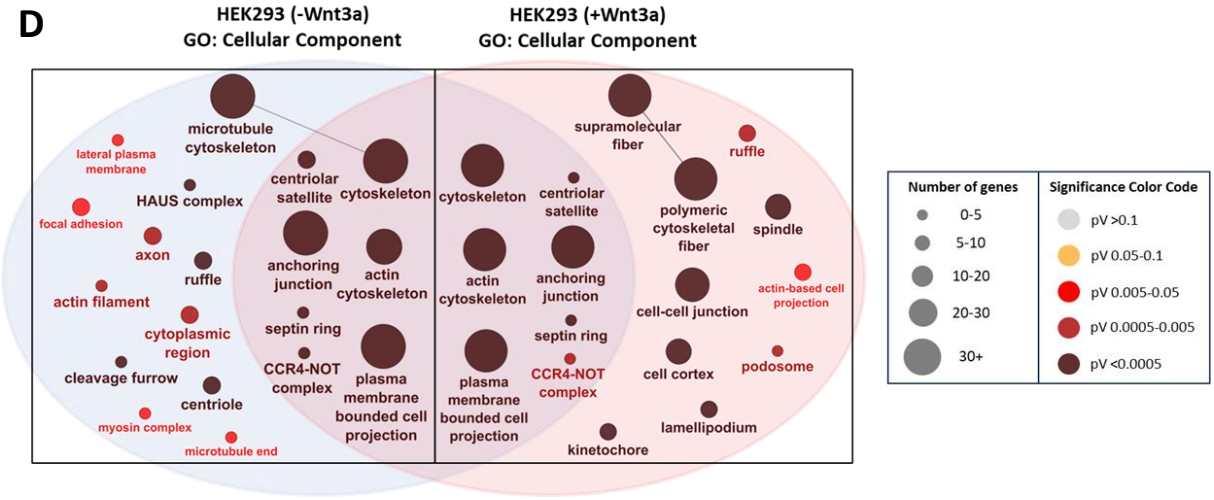
D
HEK293 (-Wnt3a)
GO: Cellular Component
HEK293 (+Wnt3a)
GO: Cellular Component
microtubule cytoskeleton
lateral plasma membrane
centriolar satellite
cytoskeleton
HAUS complex
focal adhesion
axon
ruffle
anchoring junction
actin cytoskeleton
actin filament
septin ring
cytoplasmic region
CCR4-NOT complex
cleavage furrow
centriole
plasma membrane bounded cell projection
myosin complex
microtubule end
supramolecular fiber
ruffle
polymeric cytoskeletal fiber
spindle
actin-based cell projection
cell-cell junction
cell cortex
podosome
lamellipodium
kinetochore
Number of genes
0-5
5-10
10-20
20-30
30+
Significance Color Code
pV >0.1
pV 0.05-0.1
pV 0.005-0.05
pV 0.0005-0.005
pV <0.0005

Fig. 2. Wnt3a treatment promotes IQGAP3 localization to non-membrane organelles and cell junctions. (A) IQGAP3-biotinylated proteins exclusively found in cells treated with L-cells conditioned media (-Wnt3a). Shown are proximity partners with Fold change ≥ 4, p-value ≤ 0.01, node color denote degree distribution, Created with Cytoscape. (B) IQGAP3-biotinylated proteins exclusively found in cells treated with L-Wnt3a cells conditioned media (+Wnt3a). Shown are proximity partners with Fold change ≥ 4, p-value ≤ 0.01, node color denote degree distribution, Created with Cytoscape. (C) ClueGO analysis for Biological Process enrichment of biotinylated protein in HEK293 cells treated with -Wnt3a and +Wnt3a conditioned media. Size denote number of mapped genes and node color denote p-values. (D) ClueGO analysis for Cellular Compartment enrichment of biotinylated protein in HEK293 cells treated with -Wnt3a and +Wnt3a conditioned media. Size denote number of mapped genes and node color denote p-values.

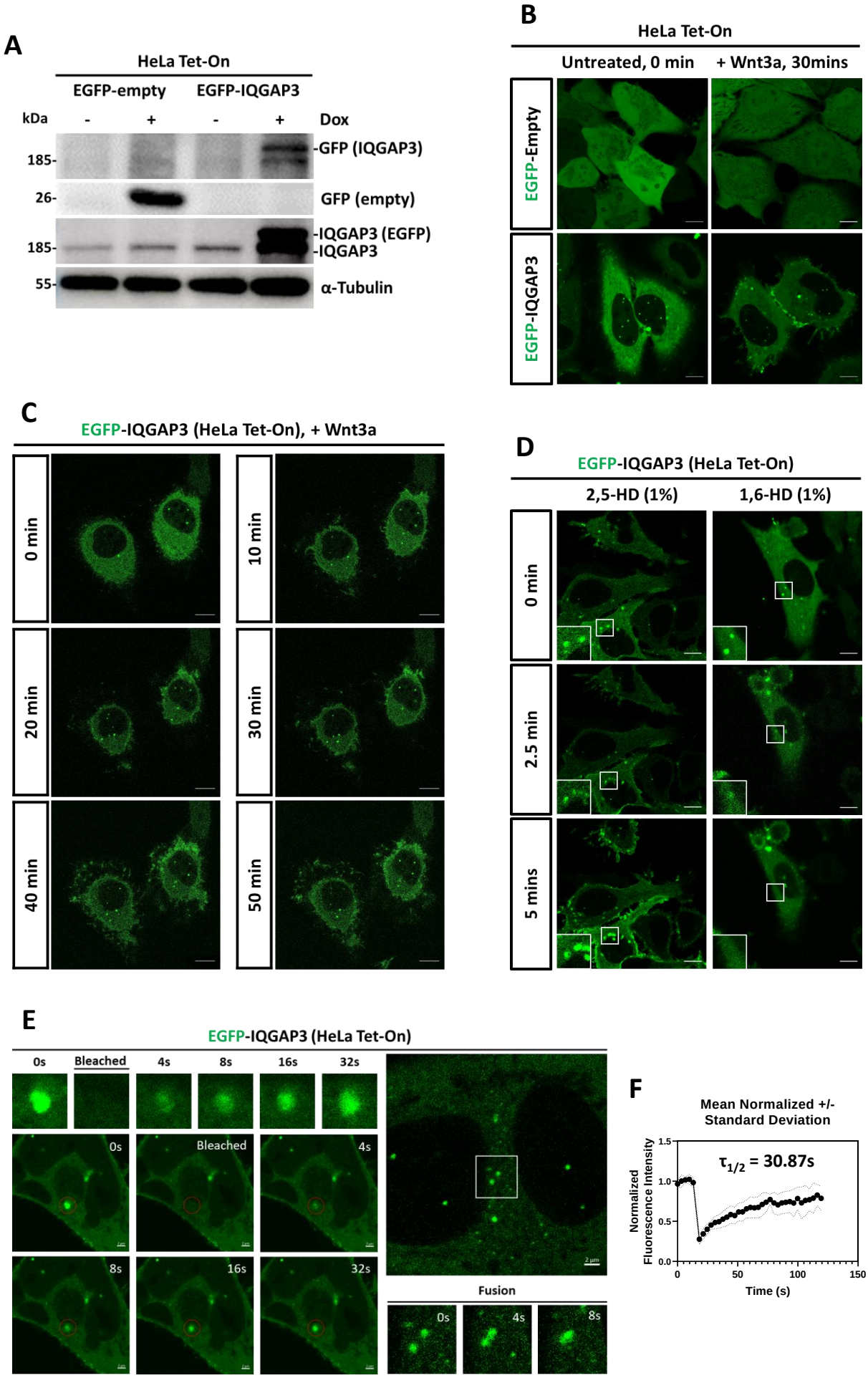
A
HeLa Tet-On
EGFP-empty
EGFP-IQGAP3
kDa
-
+
-
+
Dox
185-
-GFP (IQGAP3)
26-
GFP (empty)
185-
-IQGAP3 (EGFP)
-IQGAP3
55-
α-Tubulin
B
HeLa Tet-On
Untreated, 0 min
+ Wnt3a, 30mins
EGFP-Empty
EGFP-IQGAP3
C
EGFP-IQGAP3 (HeLa Tet-On), + Wnt3a
0 min
10 min
20 min
30 min
40 min
50 min
D
EGFP-IQGAP3 (HeLa Tet-On)
2,5-HD (1%)
1,6-HD (1%)
0 min
2.5 min
5 mins
E
EGFP-IQGAP3 (HeLa Tet-On)
0s
Bleached
4s
8s
16s
32s
Fusion
F
Mean Normalized +/-
Standard Deviation
$\tau_{1/2}$ = 30.87s
Normalized
Fluorescence Intensity
Time (s)

Fig. 3. IQGAP3 undergoes phase separation. (A) Immunoblot analysis of Doxycycline induction in HeLa Tet-On cells. Cells were induced with Doxycycline for 48 hours prior to cell lysis. (B) Live images of HeLa Tet-On cells expressing EGFP-empty and EGFP-IQGAP3 without and with Wnt3a treatment after 30 minutes. Cells were induced with Doxycycline for 48 hours prior to imaging. Images of untreated and post-treated cells are not the same cells but are the best representative examples. Scale bars, 10 µm. (C) Timelapse images of HeLa Tet-On cells expressing EGFP-IQGAP3 0 - 50 minutes post-Wnt3a treatment. Cells were induced with Doxycycline for 48 hours prior to imaging. Images of untreated and post-treated cells are the same cells (refer to timelapse video in supplementary). Scale bars, 10 µm. (D) Timelapse images of HeLa Tet-On cells expressing EGFP-IQGAP3 treated with either 1% 2,5-Hexanediol (control) or 1% 1,6-Hexanediol for 0-5 minutes. Images of untreated and post-treated cells are the same cells (refer to timelapse video in supplementary). Scale bars, 10 µm. (E) HeLa Tet-On cells stably expressing EGFP-IQGAP3 were subjected to FRAP bleaching and observed for recovery and fusion events. (For FRAP video refer to supplementary). Scale bars, 2 µm. (F) Mean normalized standard deviation of FRAP recovery of 5 bleached EGFP-IQGAP3 condensates, half time of recovery ($\tau 1/2$) = 30.87s.

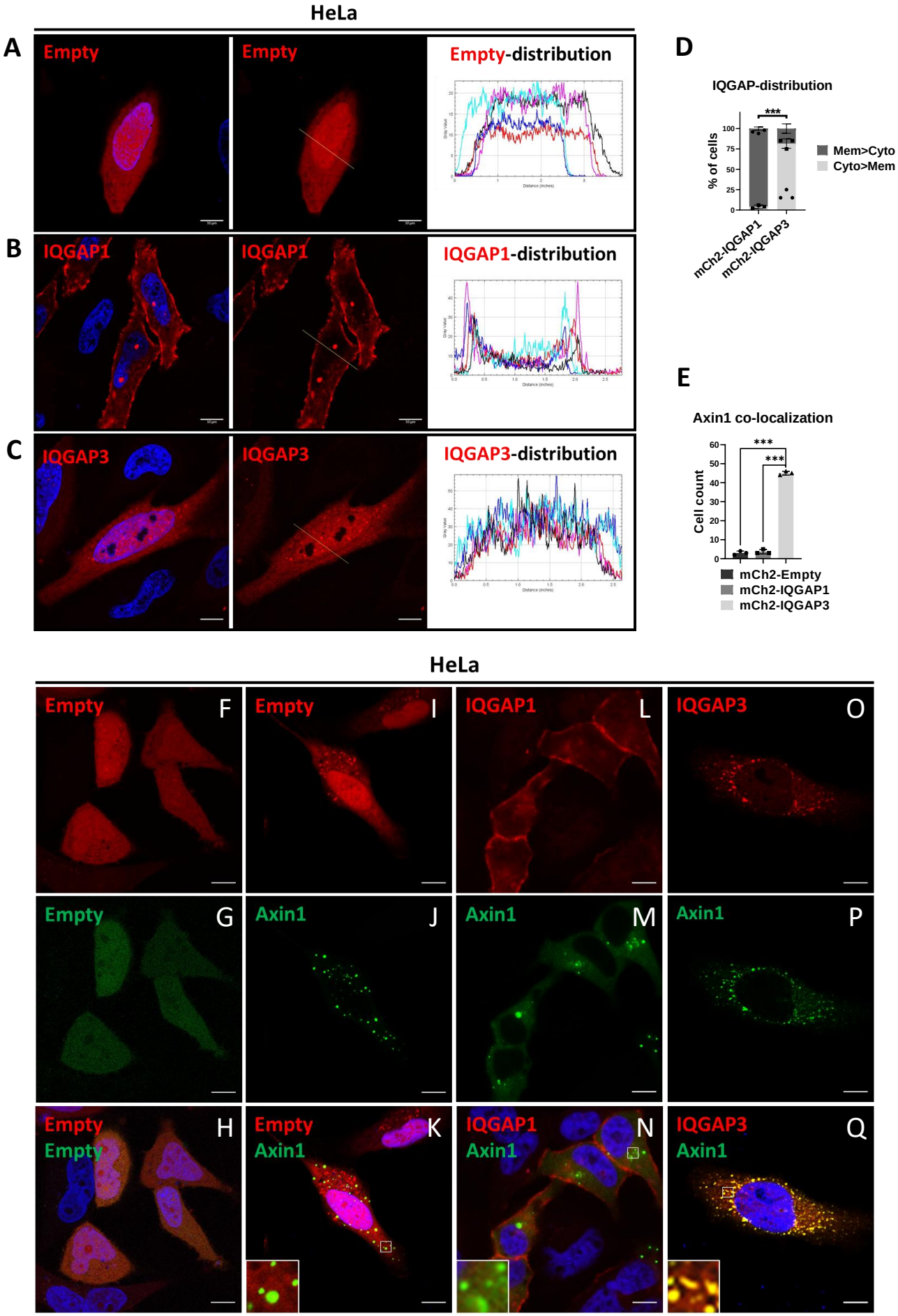
HeLa
A
Empty
Empty
Empty-distribution
B
IQGAP1
IQGAP1
IQGAP1-distribution
C
IQGAP3
IQGAP3
IQGAP3-distribution
D
IQGAP-distribution
% of cells
Mem>Cyto
Cyto>Mem
mCh2-IQGAP1
mCh2-IQGAP3
E
Axin1 co-localization
Cell count
mCh2-Empty
mCh2-IQGAP1
mCh2-IQGAP3
HeLa
Empty F
Empty I
IQGAP1 L
IQGAP3 O
Empty G
Axin1 J
Axin1 M
Axin1 P
Empty
Empty H
Empty
Axin1 K
IQGAP1
Axin1 N
IQGAP3
Axin1 Q

Fig. 4. IQGAP3 co-localizes with Axin1 puncta in the cytosol. HeLa cells were transfected with (A) mCherry2-empty and Cross-sectional line for Intensity plot measurement from 5 different cells (right). (B) mCherry-IQGAP1 and Cross-sectional line for Intensity plot measurement from 5 different cells (right). (C) mCherry2-IQGAP3 and Cross-sectional line for Intensity plot measurement from 5 different cells (right). Scale bars, 10 µm. (D) Percentile of cell count for IQGAP-distribution, cells with higher membrane intensity were counted as Membrane > Cytosol (Mem > Cyto) vice versa. Cell count for IQGAP distribution, 50 cells per sample. Representative data were collected and are expressed as the mean ± SD from three independent experiments (n=3). (E) Cell count for IQGAP-Axin1 co-localization, 50 cells per sample. Representative data were collected and are expressed as the mean ± SD from three independent experiments (n=3). Student's t test was performed, with $*p < 0.05$, $**p < 0.01$, and $***p < 0.001$. HeLa cells were transfected with (F-H) mCherry2-empty with EGFP-empty (negative control), (I-K) mCherry2-empty with EGFP-Axin1, (L-N) mCherry2-IQGAP1 with EGFP-Axin1, and (O-Q) mCherry2-IQGAP3 with EGFP-Axin1. Scale bars, 10 µm.

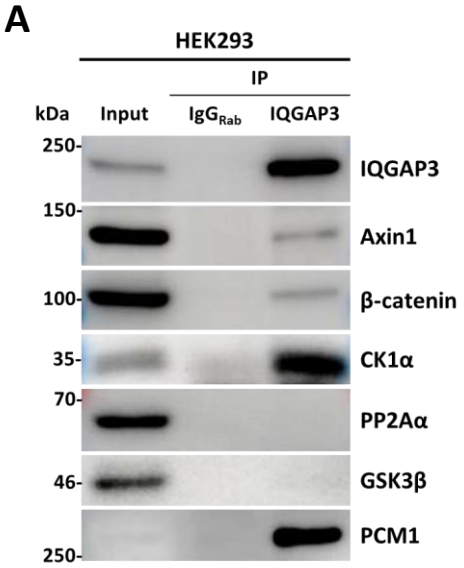
A
HEK293
IP
kDa
Input
IgG$_{Rab}$
IQGAP3
250-
150-
100-
35-
70-
46-
250-
IQGAP3
Axin1
β-catenin
CK1α
PP2Aα
GSK3β
PCM1

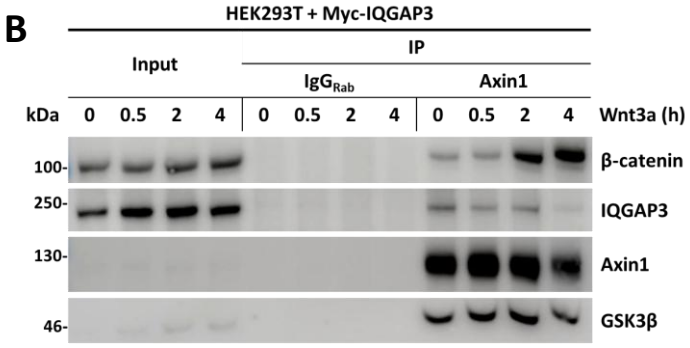
B
HEK293T + Myc-IQGAP3
Input
IP
IgG$_{Rab}$
Axin1
kDa
0 0.5 2 4 0 0.5 2 4 0 0.5 2 4
Wnt3a (h)
100-
250-
130-
46-
β-catenin
IQGAP3
Axin1
GSK3β

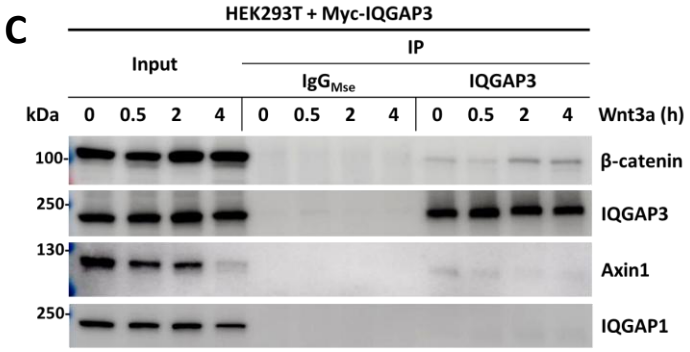
C
HEK293T + Myc-IQGAP3
Input
IP
IgG$_{Mse}$
IQGAP3
kDa
0 0.5 2 4 0 0.5 2 4 0 0.5 2 4
Wnt3a (h)
100-
250-
130-
250-
β-catenin
IQGAP3
Axin1
IQGAP1

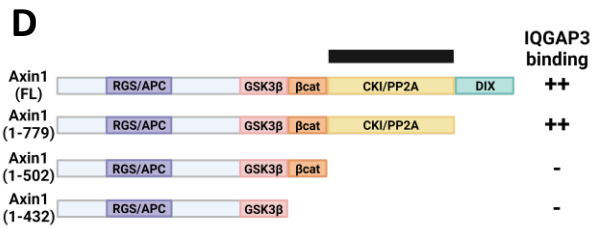
D
IQGAP3 binding
Axin1 (FL)
RGS/APC
GSK3β
βcat
CKI/PP2A
DIX
++
Axin1 (1-779)
RGS/APC
GSK3β
βcat
CKI/PP2A
++
Axin1 (1-502)
RGS/APC
GSK3β
βcat
-
Axin1 (1-432)
RGS/APC
GSK3β
-

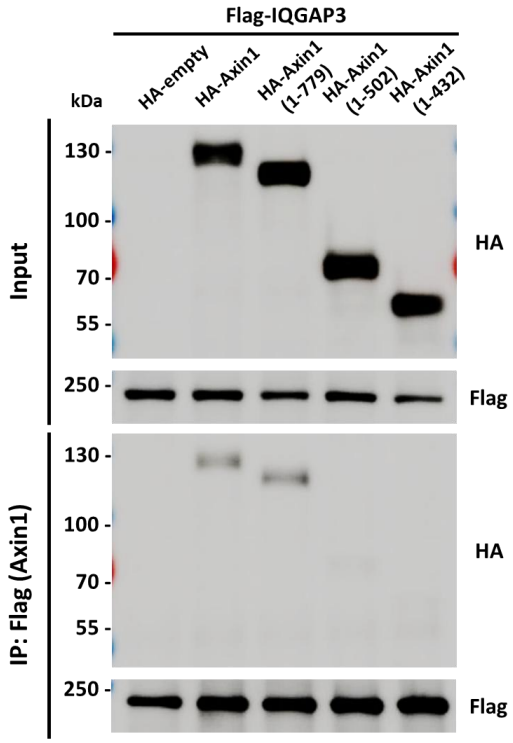
Flag-IQGAP3
kDa
HA-empty
HA-Axin1
HA-Axin1 (1-779)
HA-Axin1 (1-502)
HA-Axin1 (1-432)
Input
130 -
100 -
70 -
55 -
250 -
HA
Flag
IP: Flag (Axin1)
130 -
100 -
70 -
55 -
250 -
HA
Flag

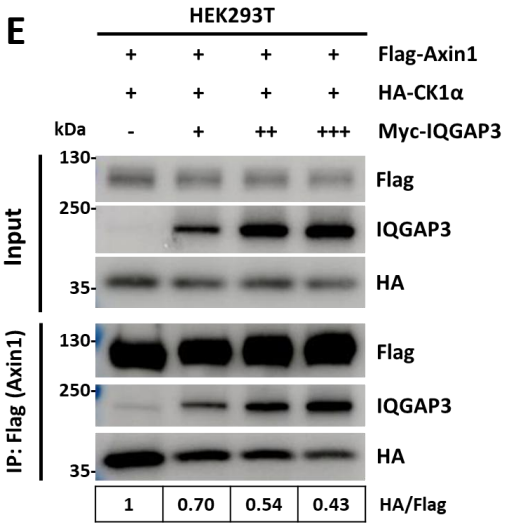
E
HEK293T
+ + + + Flag-Axin1
+ + + + HA-CK1α
kDa
- + ++ +++ Myc-IQGAP3
Input
130-
250-
35-
Flag
IQGAP3
HA
IP: Flag (Axin1)
130-
250-
35-
Flag
IQGAP3
HA
1 0.70 0.54 0.43 HA/Flag

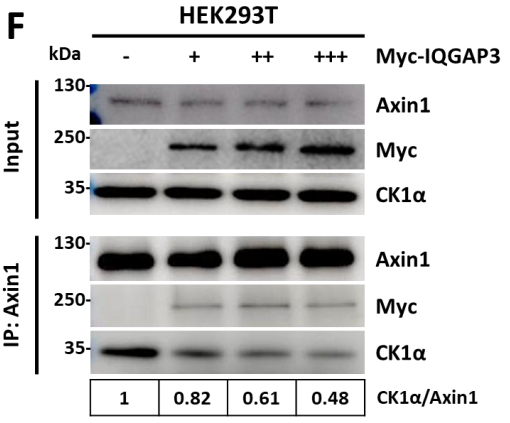
F
HEK293T
kDa
- + ++ +++ Myc-IQGAP3
Input
130-
250-
35-
Axin1
Myc
CK1α
IP: Axin1
130-
250-
35-
Axin1
Myc
CK1α
1 0.82 0.61 0.48 CK1α/Axin1

Fig. 5. IQGAP3 expression reduces Axin1-CK1α interaction. (A) Immunoblot of endogenous IQGAP3 immunoprecipitation using an IQGAP3-specific antibody (1:100) and Mouse IgG as a control, with 1 mg of HEK293 cell lysate. Samples were subjected to SDS-PAGE (7.5%) followed by immunoblotting using the indicated antibodies. (B) HEK293T cells were exposed to Wnt3a conditioned medium at different time points as indicated. Stimulated lysates were subjected to immunoprecipitation using an Axin1-specific antibody and Rabbit IgG as control and were subjected to SDS-PAGE (7.5%) followed by immunoblotting using the indicated antibodies. (C) HEK293T cells were exposed to Wnt3a conditioned medium at different time points as indicated. Stimulated lysates were subjected to IQGAP3 immunoprecipitation using Myc-Tag antibody and Mouse IgG as control and were subjected to SDS-PAGE (7.5%) followed by immunoblotting using the indicated antibodies. (D) Immunoblot of Flag-Immunoprecipitated protein expressing HA-Axin1 C-terminal truncations with Flag-IQGAP3 to map the IQGAP3 binding site within Axin1. Samples were subjected to SDS-PAGE (7.5%) followed by immunoblotting using the indicated antibodies. (E) IQGAP3 reduced exogenous Axin1-CK1 interaction. HEK293T cells expressing Flag-Axin1 were transfected with limiting amounts of HA-CK1α and increasing amounts of Myc-IQGAP3 (5μg/10μg/15μg) as indicated, and the lysates were subjected to anti-Flag immunoprecipitation. Samples were subjected to SDS-PAGE (7.5%) followed by immunoblotting using the indicated antibodies. The relative immunoblot bands of HA and Flag (HA/Flag) from the immunoprecipitation membrane were quantified by densitometry. (F) IQGAP3 reduced endogenous Axin1-CK1 interaction. HEK293T cells were transfected with increasing amounts of Myc-IQGAP3 (5μg/10μg/15μg) as indicated, and the lysates were subjected to anti-Axin1 immunoprecipitation. Samples were subjected to SDS-PAGE (10%) followed by immunoblotting using the indicated antibodies. The relative immunoblot bands of CK1α and Axin1 (CK1α/Axin1) from the immunoprecipitation membrane were quantified by densitometry.

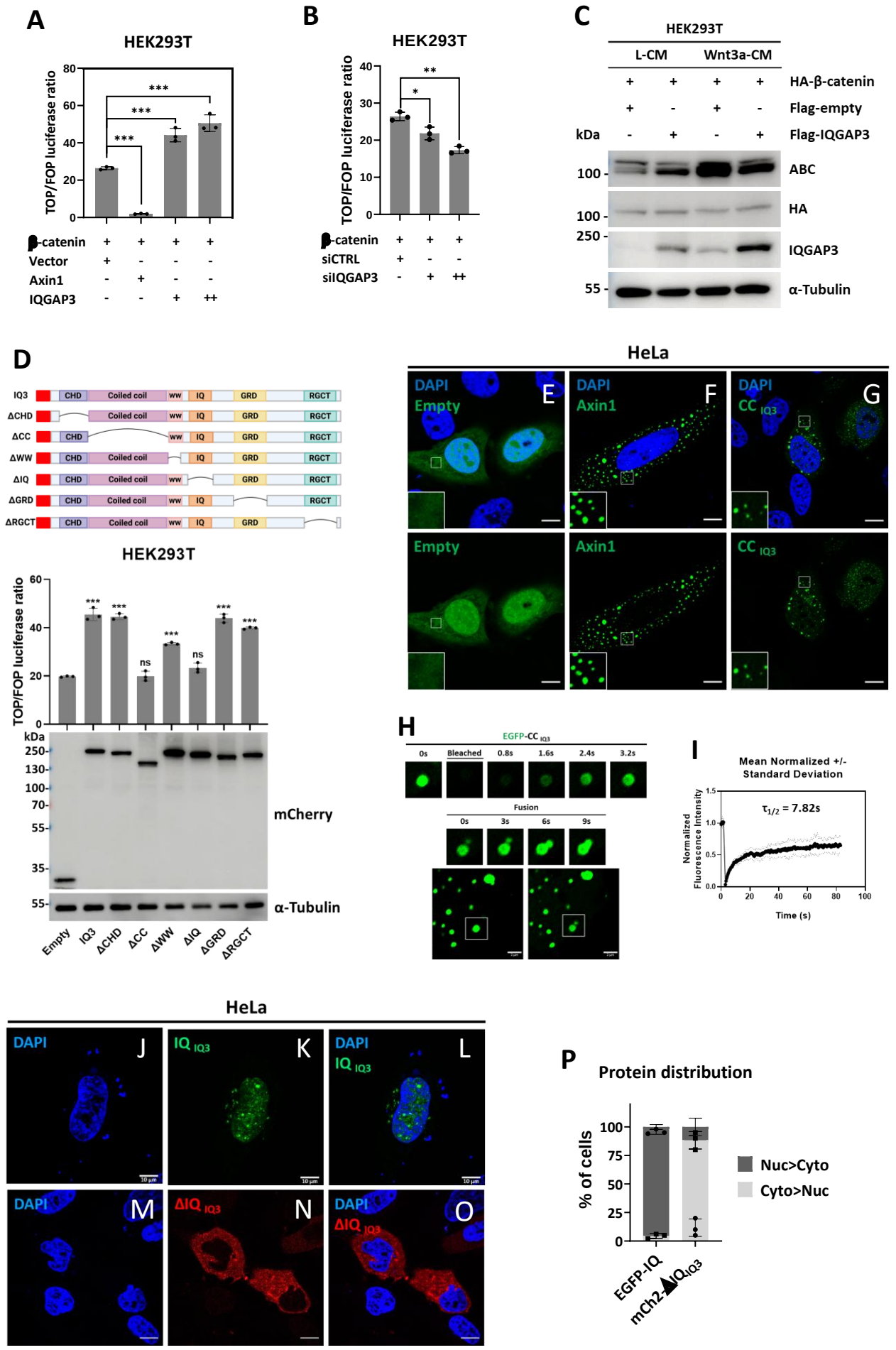
A
HEK293T
TOP/FOP luciferase ratio
β-catenin
Vector
Axin1
IQGAP3
B
HEK293T
TOP/FOP luciferase ratio
β-catenin
siCTRL
siIQGAP3
C
HEK293T
L-CM
Wnt3a-CM
HA-β-catenin
Flag-empty
Flag-IQGAP3
kDa
ABC
HA
IQGAP3
α-Tubulin
D
IQ3
ΔCHD
ΔCC
ΔWW
ΔIQ
ΔGRD
ΔRGCT
CHD
Coiled coil
WW
IQ
GRD
RGCT
HEK293T
TOP/FOP luciferase ratio
mCherry
α-Tubulin
Empty
HeLa
DAPI
Empty
Axin1
CC IQ3
E
F
G
H
EGFP-CC IQ3
0s
Bleached
0.8s
1.6s
2.4s
3.2s
Fusion
3s
6s
9s
I
Mean Normalized +/- Standard Deviation
Normalized Fluorescence Intensity
Time (s)
HeLa
IQ IQ3
ΔIQ IQ3
J
K
L
M
N
O
P
Protein distribution
% of cells
Nuc>Cyto
Cyto>Nuc
EGFP-IQ
mCh2-ΔIQ IQ3

Fig. 6. IQGAP3 promotes β-catenin activity through its CC and IQ domains. (A) TOPFlash assay of β-catenin co-overexpression with Axin1 or increasing IQGAP3 (300μg, 600μg) in HEK293T cells. The data is representative of three independent experiments. Student's t test was performed, with $*p < 0.05$, $**p < 0.01$, and $***p < 0.001$. (B) TOPFlash assay of β-catenin co-overexpression with siControl or increasing siIQGAP3 (20nM, 50nM) in HEK293T cells. The data is representative of three independent experiments. Student's t test was performed, with $*p < 0.05$, $**p < 0.01$, and $***p < 0.001$. (C) Immunoblot of IQGAP3 overexpression with and without Wnt3a conditioned media treatment. The data is representative of three independent experiments. (D) TOPFlash and Immunoblot assays of β-catenin overexpression with a series of IQGAP3 domain deletions. The data is representative of three independent experiments. HeLa cells transfected with (E) EGFP-empty, (F) EGFP-Axin1, and (G) EGFP-CC. Scale bars, 10 μm. (H) HeLa cells were transfected with EGFP-CC, subjected to FRAP bleaching, and observed for recovery and fusion events. Scale bars, 2μm. (I) Mean normalized standard deviation of FRAP recovery of 10 bleached EGFP-CC condensates, half time of recovery ($\tau 1/2$) = 7.82s. HeLa cells transfected with (J-L) EGFP-IQ domain and (M-O) mCherry2-IQGAP3ΔIQ. Scale bars, 10 μm. (P) Percentile of cell count for protein distribution, cells with higher nuclear intensity were counted as Nuclear > Cytosol (Nuc > Cyto), vice versa. Cell count for protein distribution, 50 cells per sample. Representative data were collected and are expressed as the mean ± SD from three independent experiments (n=3).

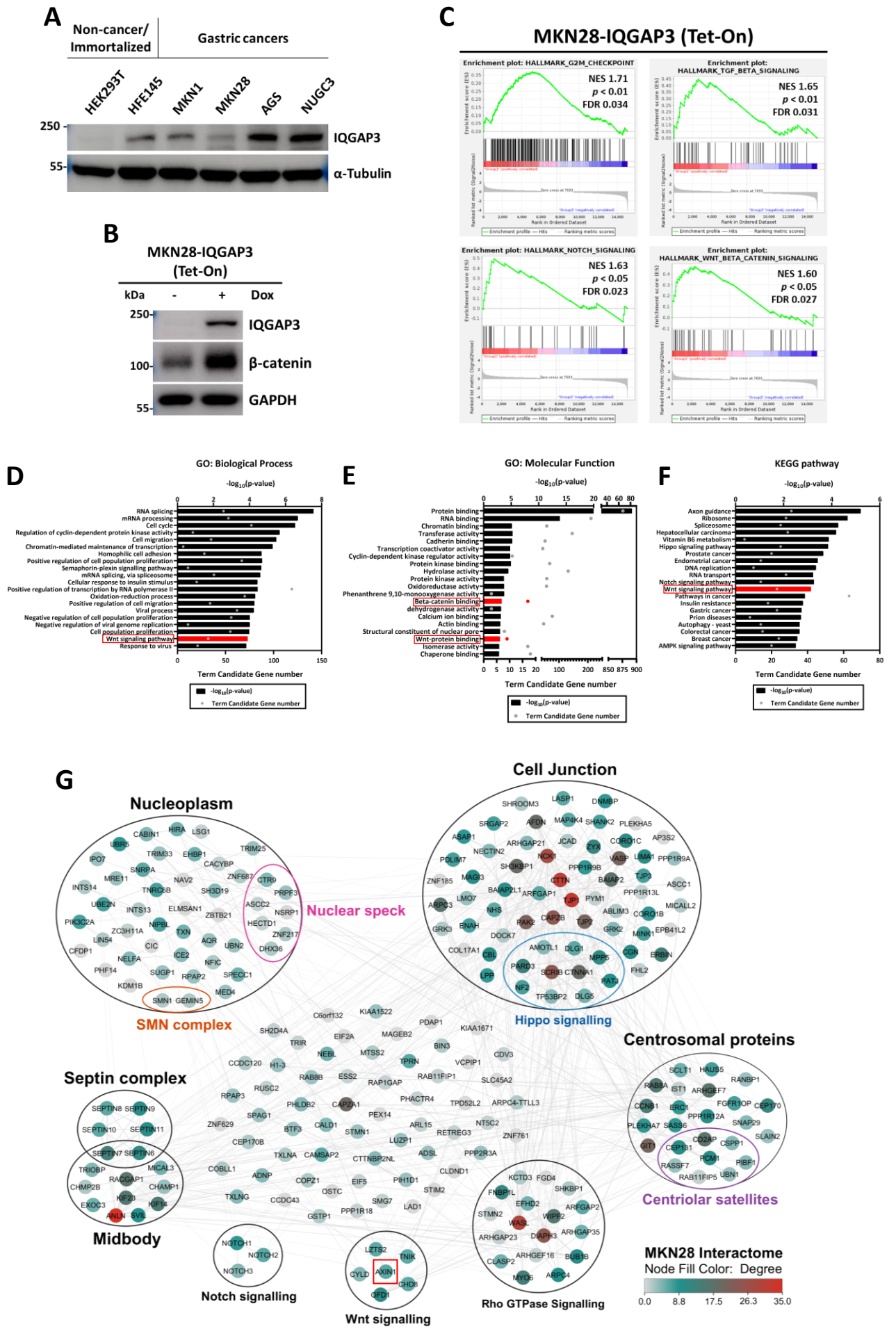
A
Non-cancer/ Immortalized
Gastric cancers
HEK293T
HFE145
MKN1
MKN28
AGS
NUGC3
250 -
IQGAP3
55-
α-Tubulin
B
MKN28-IQGAP3 (Tet-On)
kDa
-
+
Dox
250-
IQGAP3
100-
β-catenin
55-
GAPDH
C
MKN28-IQGAP3 (Tet-On)
Enrichment plot: HALLMARK_G2M_CHECKPOINT
NES 1.71
p < 0.01
FDR 0.034
Enrichment plot: HALLMARK_TGF_BETA_SIGNALING
NES 1.65
p < 0.01
FDR 0.031
Enrichment plot: HALLMARK_NOTCH_SIGNALING
NES 1.63
p < 0.05
FDR 0.023
Enrichment plot: HALLMARK_WNT_BETA_CATENIN_SIGNALING
NES 1.60
p < 0.05
FDR 0.027
D
GO: Biological Process
-log10(p-value)
RNA splicing
mRNA processing
Cell cycle
Regulation of cyclin-dependent protein kinase activity
Cell migration
Chromatin-mediated maintenance of transcription
Homophilic cell adhesion
Positive regulation of cell population proliferation
Semaphorin-plexin signalling pathway
mRNA splicing, via spliceosome
Cellular response to insulin stimulus
Positive regulation of transcription by RNA polymerase II
Oxidation-reduction process
Positive regulation of cell migration
Viral process
Negative regulation of cell population proliferation
Negative regulation of viral genome replication
Cell population proliferation
Wnt signaling pathway
Response to virus
Term Candidate Gene number
-log10(p-value)
Term Candidate Gene number
E
GO: Molecular Function
-log10(p-value)
Protein binding
RNA binding
Chromatin binding
Transferase activity
Cadherin binding
Transcription coactivator activity
Cyclin-dependent kinase regulator activity
Protein kinase binding
Hydrolase activity
Protein kinase activity
Oxidoreductase activity
Phenanthrene 9,10-monooxygenase activity
Beta-catenin binding
dehydrogenase activity
Calcium ion binding
Actin binding
Structural constituent of nuclear pore
Wnt-protein binding
Isomerase activity
Chaperone binding
Term Candidate Gene number
-log10(p-value)
Term Candidate Gene number
F
KEGG pathway
-log10(p-value)
Axon guidance
Ribosome
Spliceosome
Hepatocellular carcinoma
Vitamin B6 metabolism
Hippo signaling pathway
Prostate cancer
Endometrial cancer
DNA replication
RNA transport
Notch signaling pathway
Wnt signaling pathway
Pathways in cancer
Insulin resistance
Gastric cancer
Prion diseases
Autophagy - yeast
Colorectal cancer
Breast cancer
AMPK signaling pathway
Term Candidate Gene number
-log10(p-value)
Term Candidate Gene number
G
Nucleoplasm
Nuclear speck
SMN complex
Cell Junction
Hippo signalling
Centrosomal proteins
Centriolar satellites
Septin complex
Midbody
Notch signalling
Wnt signalling
Rho GTPase Signalling
MKN28 Interactome
Node Fill Color: Degree
0.0
8.8
17.5
26.3
35.0

Fig. 7. IQGAP3 overexpression increases β-catenin levels in MKN28 cells. (A) Immunoblot of non-cancer/immortalized (HEK293T and HFE145) and gastric cancer cell lines (MKN1, AGS, and NUGC3). Samples were subjected to SDS-PAGE (7.5%) followed by immunoblotting using the indicated antibodies. (B) Immunoblot of MKN28 cells expressing doxycycline-inducible 3×Flag-IQGAP3. Samples were subjected to SDS-PAGE (7.5%) followed by immunoblotting using the indicated antibodies. (C) GSEA data from RNA-seq of IQGAP3 overexpression in MKN28 cells, showing top 4 pathways. (D) Gene ontology: Biological Process Enrichment histogram of RNA-seq data from IQGAP3 overexpression in MKN28 cells. Wnt Signaling pathway represented with red bar. (E) Gene ontology: Molecular function Enrichment histogram of RNA-seq data from IQGAP3 overexpression in MKN28 cells. Wnt-protein and beta-catenin binding are represented with red bars. (F) KEGG pathway Enrichment histogram of RNA-seq data from IQGAP3 overexpression in MKN28 cells. Wnt Signaling pathway represented with red bar. (G) IQGAP3 interactome mapped from MKN28 cells stably expressing doxycycline-inducible TurboID-IQGAP3 (Fold change ≥ 2, p-value ≤ 0.05), node color denote degree distribution, Created with Cytoscape.

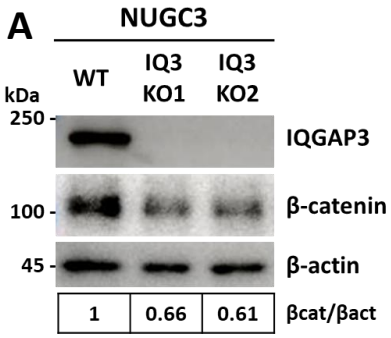
A
NUGC3
WT
IQ3 KO1
IQ3 KO2
kDa
250
100
45
IQGAP3
β-catenin
β-actin
1
0.66
0.61
βcat/βact

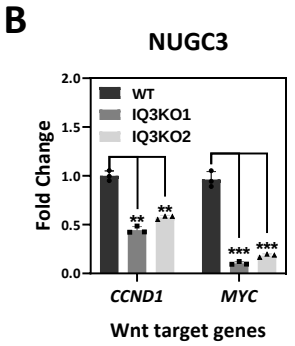
B
NUGC3
WT
IQ3KO1
IQ3KO2
Fold Change
2.0
1.5
1.0
0.5
0.0
CCND1
MYC
Wnt target genes

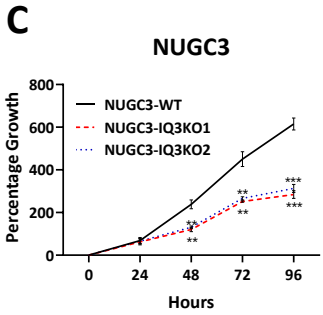
C
NUGC3
NUGC3-WT
NUGC3-IQ3KO1
NUGC3-IQ3KO2
Percentage Growth
800
600
400
200
0
0
24
48
72
96
Hours

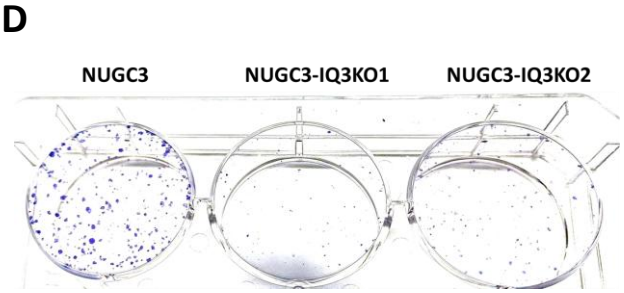
D
NUGC3
NUGC3-IQ3KO1
NUGC3-IQ3KO2

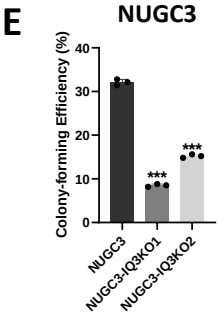
E
NUGC3
Colony-forming Efficiency (%)
40
30
20
10
0
NUGC3
NUGC3-IQ3KO1
NUGC3-IQ3KO2

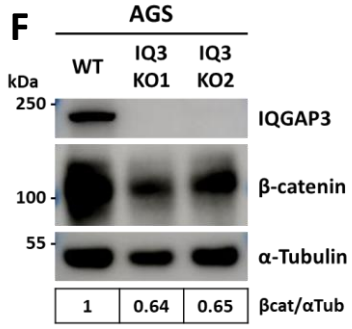
F
AGS
WT
IQ3 KO1
IQ3 KO2
kDa
250
100
55
IQGAP3
β-catenin
α-Tubulin
1
0.64
0.65
βcat/αTub

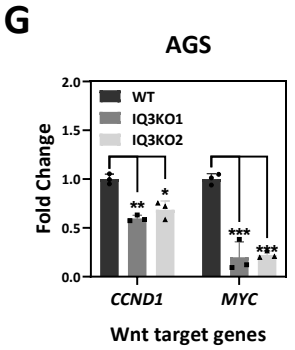
G
AGS
WT
IQ3KO1
IQ3KO2
Fold Change
2.0
1.5
1.0
0.5
0.0
CCND1
MYC
Wnt target genes

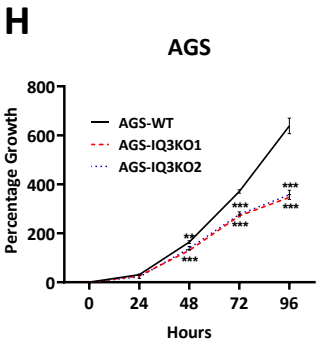
H
AGS
AGS-WT
AGS-IQ3KO1
AGS-IQ3KO2
Percentage Growth
800
600
400
200
0
0
24
48
72
96
Hours

I
AGS
AGS-IQ3KO1
AGS-IQ3KO2

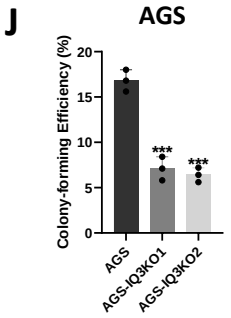
J
AGS
Colony-forming Efficiency (%)
20
15
10
5
0
AGS
AGS-IQ3KO1
AGS-IQ3KO2

Fig. 8. Loss of IQGAP3 reduces β-catenin levels in NUGC3 and AGS cells. (A) Immunoblot of NUGC3 wild-type and IQGAP3 CRISPR knock-out clones. Samples were subjected to SDS-PAGE (7.5%) followed by immunoblotting using the indicated antibodies. The relative immunoblot bands of β-catenin and β-actin (βcat/βact) were quantified by densitometry. (B) NUGC3 cells were lysed, and RNA collected were converted to cDNA and subjected to RT-PCR to quantify the amount of Wnt target genes *CCND1* and *MYC.* Representative data were collected and are expressed as the mean ± SD from three independent experiments. Student's t test was performed, with $*p < 0.05$, $**p < 0.01$, and $***p < 0.001$. (C) XTT Cell Proliferation Assay of NUGC3 wild-type and IQGAP3 CRISPR knock-out clones. Representative data were collected and are expressed as the mean % growth ± SD from three independent experiments. Two-way ANOVA was performed, with $*p < 0.05$, $**p < 0.01$, and $***p < 0.001$. (D) Clonogenic Assay of NUGC3 wild-type and IQGAP3 CRISPR knock-out clones. (E) Colony-Forming Efficiency (%) of NUGC3 wild-type and IQGAP3 CRISPR knock-out clones. (F) Immunoblot of AGS wild-type and IQGAP3 CRISPR knock-out clones. Image is best representative of three independent experiments. Samples were subjected to SDS-PAGE (7.5%) followed by immunoblotting using the indicated antibodies. The relative immunoblot bands of β-catenin and α-Tubulin (βcat/αTub) were quantified by densitometry. (G) AGS cells were lysed, and RNA collected were converted to cDNA and subjected to RT-PCR to quantify the amount of Wnt target genes *CCND1* and *MYC.* Representative data were collected and are expressed as the mean ± SD from three independent experiments. Student's t test was performed, with $*p < 0.05$, $**p < 0.01$, and $***p < 0.001$. (H) XTT Cell Proliferation Assay of AGS wild-type and IQGAP3 CRISPR knock-out clones. Representative data were collected and are expressed as the mean % growth ± SD from three independent experiments. Two-way ANOVA was performed, with $*p < 0.05$, $**p < 0.01$, and $***p < 0.001$. (I) Clonogenic Assay of AGS wild-type and IQGAP3 CRISPR knock-out clones. (J) Colony-Forming Efficiency (%) of AGS wild-type and IQGAP3 CRISPR knock-out clones.

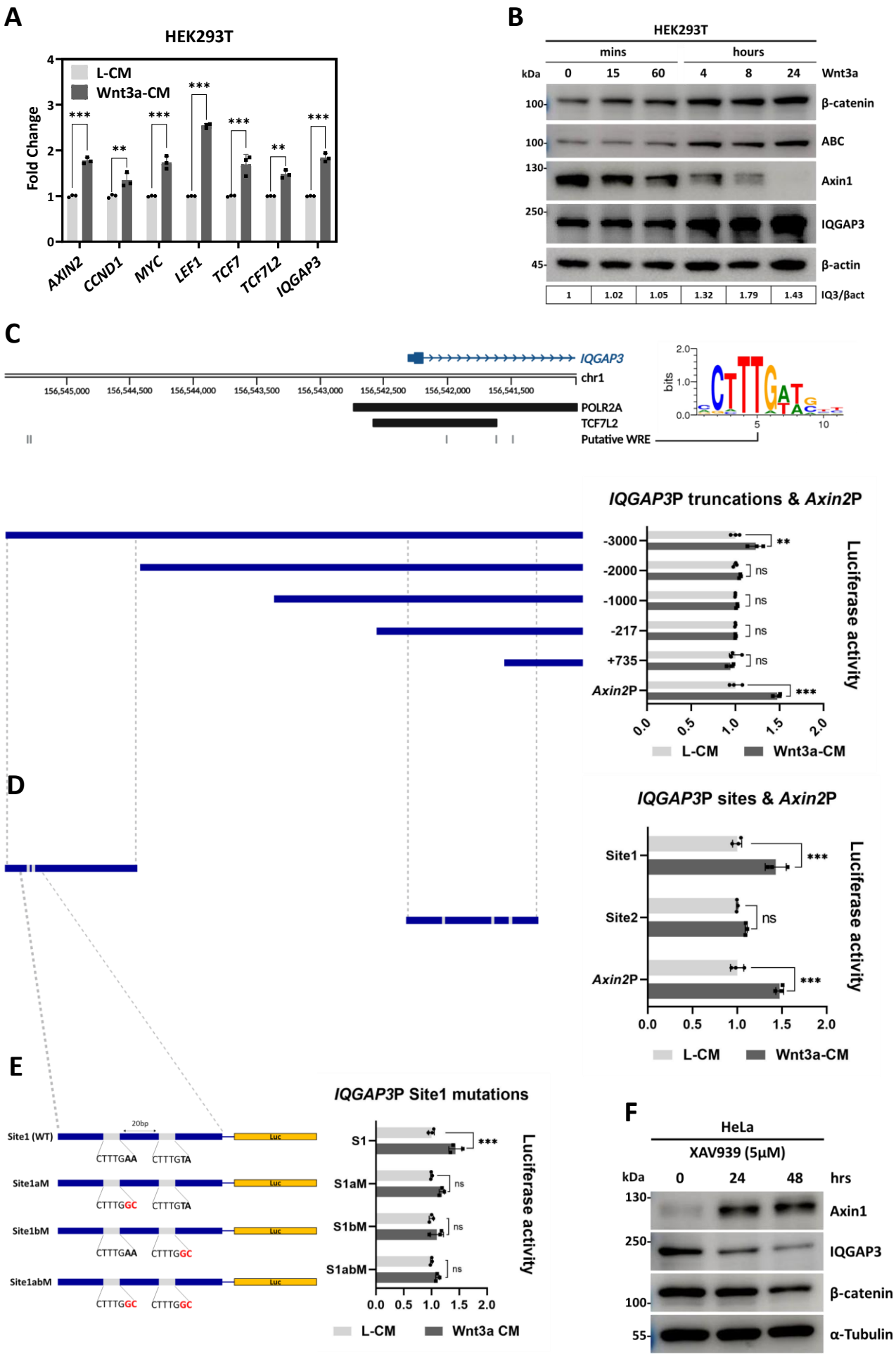
A
HEK293T
L-CM
Wnt3a-CM
Fold Change
AXIN2
CCND1
MYC
LEF1
TCF7
TCF7L2
IQGAP3
B
HEK293T
mins
hours
kDa
0
15
60
4
8
24
Wnt3a
β-catenin
ABC
Axin1
IQGAP3
β-actin
IQ3/βact
1
1.02
1.05
1.32
1.79
1.43
C
IQGAP3
chr1
POLR2A
TCF7L2
Putative WRE
bits
D
IQGAP3P truncations & Axin2P
-3000
-2000
-1000
-217
+735
Axin2P
ns
Luciferase activity
L-CM
Wnt3a-CM
IQGAP3P sites & Axin2P
Site1
Site2
E
IQGAP3P Site1 mutations
Site1 (WT)
Site1aM
Site1bM
Site1abM
20bp
Luc
CTTTGAA
CTTTGTA
CTTTGC
CTTTGGC
S1
S1aM
S1bM
S1abM
Wnt3a CM
F
HeLa
XAV939 (5μM)
hrs
Axin1
IQGAP3
β-catenin
α-Tubulin

Fig. 9. IQGAP3 is a target of Wnt signaling, sustains Wnt signaling via a positive feedback loop. (A) HEK293T cells were treated with wnt3a conditioned media supplemented with 100ng/ml of rhWnt3a. Cells were harvested, and the RNA collected were converted to cDNA and subjected to RT-PCR to quantify the amount of *AXIN2, CCND1, MYC, LEF1, TCF7, TCF7L2* and *IQGAP3* transcripts levels. (B) Time-course of HEK293T cells treated with Wnt3a conditioned media supplemented with 100ng/ml of rhWnt3a. Image is best representative of three independent experiments. Samples were subjected to SDS-PAGE (7.5%) followed by immunoblotting using the indicated antibodies. The relative immunoblot bands of IQGAP3 and β-actin (IQ3/βact) were quantified by densitometry. (C) Luciferase assay of 5' truncation of IQGAP3 promoter region upon treatment with L-cells conditioned or wnt3a conditioned media. (D) Luciferase assay of Site1 and Site2 within the IQGAP3 promoter region upon treatment with L-cells conditioned or wnt3a conditioned media. (E) Luciferase assay of Site1, Site1a mutant, Site1b mutant and Site1ab mutant upon treatment with L-cells conditioned or wnt3a conditioned media. (F) Time-course of HeLa cells treated with 5μM of XAV939. Samples were subjected to SDS-PAGE (7.5%) followed by immunoblotting using the indicated antibodies. All the above data are representative of three independent experiments.

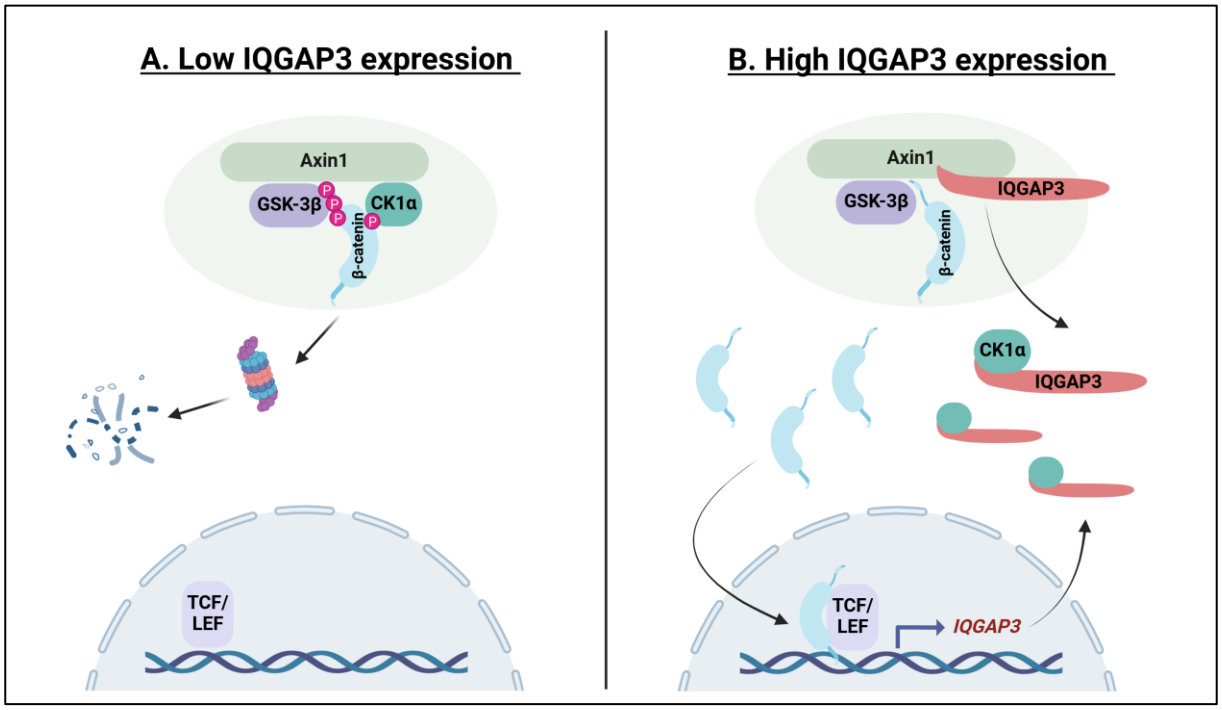
A. Low IQGAP3 expression
Axin1
GSK-3β
CK1α
P
β-catenin
TCF/
LEF
B. High IQGAP3 expression
Axin1
IQGAP3
GSK-3β
β-catenin
CK1α
IQGAP3
TCF/
LEF
IQGAP3

Fig. 10: Proposed model for IQGAP3 role in Wnt signalling. We proposed that In IQGAP3-low cells (A), the destruction complex phosphorylates β-catenin, targeting it for degradation. Meanwhile, in IQGAP3-high cells (B), IQGAP3 competes with CK1α for binding to Axin1 or sequesters it away from Axin1 or both, thus, inhibiting CK1α-mediated β-catenin phosphorylation. This inhibition leads to the accumulation of β-catenin, which promotes the expression of Wnt target genes, including IQGAP3, Created with BioRender.com.